Streamflow observations from cameras: large scale particle image velocimetry or particle tracking velocimetry?

F. Tauro[1] , R. Piscopia[1], and S. Grimaldi[1,2]

[1]University of Tuscia, Department for Innovation in Biological, Agro-food and Forest systems, Viterbo 01100, Italy

[2]New York University Tandon School of Engineering, Department of Mechanical and Aerospace Engineering, Brooklyn 11201, NY USA

Key Points:

- Image-based streamflow observations are rarely implemented in practice due to Large Scale Particle Image Velocimetry sensitivity to tracers
- Applied to images in controlled conditions and from a gauge-cam, LSPIV underestimates velocity while PTV is in agreement with benchmark data
- A modified PTV that implements a trajectory-based filtering procedure offers tangible data to evaluate the accuracy of velocity estimations

Corresponding author: Salvatore Grimaldi, `salvatore.grimaldi@unitus.it`

This article has been accepted for publication and undergone full peer review but has not been through the copyediting, typesetting, pagination and proofreading process which may lead to differences between this version and the Version of Record. Please cite this article as an 'Accepted Article', doi: 10.1002/2017WR020848

Abstract

Image-based methodologies, such as large scale particle image velocimetry (LSPIV) and particle tracking velocimetry (PTV), have increased our ability to noninvasively conduct streamflow measurements by affording spatially distributed observations at high temporal resolution. However, progress in optical methodologies has not been paralleled by the implementation of image-based approaches in environmental monitoring practice. We attribute this fact to the sensitivity of LSPIV, by far the most frequently adopted algorithm, to visibility conditions and to the occurrence of visible surface features. In this work, we test both LSPIV and PTV on a data set of 12 videos captured in a natural stream wherein artificial floaters are homogeneously and continuously deployed. Further, we apply both algorithms to a video of a high flow event on the Tiber River, Rome, Italy. In our application, we propose a modified PTV approach that only takes into account realistic trajectories. Based on our findings, LSPIV largely underestimates surface velocities with respect to PTV in both favorable (12 videos in a natural stream) and adverse (high flow event in the Tiber River) conditions. On the other hand, PTV is in closer agreement than LSPIV with benchmark velocities in both experimental settings. In addition, the accuracy of PTV estimations can be directly related to the transit of physical objects in the field of view, thus providing tangible data for uncertainty evaluation.

1 Introduction

Streamflow data are essential for developing and calibrating rainfall-runoff models. In most open-channels, discharge estimations are conducted with the velocity-area method, which is based on discrete integration of discharge from flow velocity and depth measurements sampled throughout the channel cross-section [*LeCoz et al.*, 2012; *International Organization for Standardization*, 2007a,b]. In individual surveys, velocity measurements are conducted with rotating propellers lowered into the stream at different depths and stabilized with weights [*International Organization for Standardization*, 2007a]. However, since direct velocity and depth measurements are expensive and time-consuming, such surveys are performed once every several years depending on site complexity, existing number of gaugings, and funding availability. In turn, discharge is routinely derived from curves relating water level to flow, that is, rating curves [*Clarke*, 1999]. Errors in water level and velocity measurements during surveys and cross-section change due to vegetation growth and bed movement have been regarded as considerable sources of uncertainties in discharge measurements through rating curves [*McMillan et al.*, 2010]. Another considerable source of uncertainty is due to the fact that individual surveys at selected cross-sections are conducted during low to moderate flow conditions to limit safety hazards to operators and instrumentation. In fact, during floods, the use of rotating propellers may be hindered or lead to considerable errors due to the transit of debris and bulky stones or tree trunks [*Costa et al.*, 2000]. Therefore, rating curves are rarely adequate to evaluate discharge in severe flood and drought conditions [*DiBaldassarre and Montanari*, 2009], and they hamper the accuracy of flood-frequency and flood-inundated areas estimations.

The use of acoustic Doppler current profilers (ADCPs) has partially mitigated the issues of updating rating curves and gathering measurements in moderate flood conditions [*Yorke and Oberg*, 2002; *International Organization for Standardization*, 2012]. In fact, ADCPs enable the simultaneous acquisition of water velocity and river depth [*Mueller et al.*, 2013]. Measurements can be conducted with small boats along river transects, whereby profiling each transect typically takes 30 min, or by installing the profiler on the channel bed. Alternatively, instruments can be installed horizontally at a river bank, and continuous discharge data can be obtained from single-depth horizontal array observations of velocity [*Hoitink et al.*, 2009]. This methodology is promising for estimating discharge in wide rivers (that is, from a few to several tens of meters); however, the approach is affected by river bed morphology and flow turbulence [*Mueller et al.*, 2013]. Fixed ADCPs enable measurements during high flows, yet, their use presents issues in case of cross-section change [*Le Coz et al.*, 2008]. Therefore, mobile ADCPs would be required for updating rating curves [*Le Coz et al.*, 2016]. In addition, the sensor needs to be in contact with the current and is relatively expensive, thus preventing its use in severe flood conditions.

Non-contact flow sensing approaches present several advantages with respect to traditional methodologies. Instruments are not lowered into the stream, thus limiting flow disturbance and damages during floods. In *Costa et al.* [2000], a proof of concept experiment was performed by measuring river surface velocity with a pulsed doppler radar and channel cross-sectional area with a ground-penetrating radar antenna. Mean cross-sectional velocity was estimated assuming a typical velocity profile for the channel. Further applications of radar technology can be found in *Melcher et al.* [2002] and *Costa et al.* [2006]. Similar noninvasive approaches entail the use of X-band radars [*Lee et al.*, 2002], coherent microwave systems [*Plant et al.*, 2005], and thermal infrared imagery [*Puleo et al.*, 2012].

Despite their promise, these methodologies are rarely implemented in environmental monitoring practice due to costs.

In the last decades, streamflow gauging in remote areas has also been attempted with satellite altimetry [*Koblinsky et al.*, 1993]. Satellite observations of river level are typically retrieved from radar altimeters and combined with ground measurements and satellite data, such as cross-section geometry or velocity measurements, to estimate river discharge and inundation areas [*Smith*, 1997; *Tarpanelli et al.*, 2013, 2015]. Satellite observations have also been instrumental for hydraulic model calibration [*Domeneghetti et al.*, 2014; *Domeneghetti*, 2016] and flood propagation modeling [*Yan et al.*, 2015]. Recently, a fully noninvasive method based on Landsat Thematic Mapper images has been demonstrated to estimate absolute discharges of large scale rivers agreeing to within $20-30\%$ of traditional in situ measurements [*Gleason and Smith*, 2014]. Ongoing and future satellite-based observations, such as measurements enabled by the Surface Water & Ocean Topography (SWOT) mission, are expected to open novel avenues in streamflow measurements. However, currently, satellite resolution and turn-around times present serious challenges in discharge estimation. Even if water level time series have been densified by considering multimission satellite data [*Tourian et al.*, 2016], altimetry data have only been recently applied for monitoring rivers smaller than several hundreds of meters in width with typical errors from 30 to 70 cm and the use of such data still requires sophisticated processing [*Schumann and Domeneghetti*, 2016].

Both invasive and non-contact traditional streamflow gauging technologies tend to be expensive, and, with the exception of satellite-based data, present limited spatial coverage [*Gleick*, 1998; *Hannah et al.*, 2011]. Dealing with costly equipment involves maintenance of sophisticated technology and adequately trained staff [*Turnipseed and Sauer*, 2010]. Such difficulties hinder the implementation of dense sensing networks in difficult-to-access environments [*van de Giesen et al.*, 2014]. Optical methods based on the acquisition of digital images of the stream surface have been a promising opportunity for inexpensive and noninvasive streamflow monitoring. Image-based approaches rely on the use of low-cost commercial cameras, and information on stream surface velocity is inferred by applying a multitude of diverse algorithms. Popular velocimetry approaches involve the analysis of digital images with large scale particle image velocimetry (LSPIV) and particle tracking velocimetry (PTV). However, alternative methods, such as the space-time image velocimetry [*Fujita et al.*, 2007] and dimensionality-reduction algorithms [*Tauro et al.*, 2014a], have also been used to gather information on flow regime from images.

Images afford noninvasive and spatially distributed observations of surface stream velocities at high temporal resolution. Their use has been demonstrated in diverse experimental settings. For instance, image-based methods work well in case of shallow flows, where alternative equipment is not applicable [*Weitbrecht et al.*, 2002; *Meselhe et al.*, 2004]. Also, they enable flow field measurements rather than point-wise estimations. Image-based approaches, such as LSPIV, have been successfully adopted to reconstruct rating curves and estimate discharge in riverine systems [*Hauet et al.*, 2008a]. Further, due to inexpensive digital image storage, measurement stations based on the continuous acquisition of frames have been established to monitor streamflow regime over long time spans [*Kim*, 2006; *Tauro et al.*, 2016a]. Finally, aircrafts and unmanned aerial vehicles have been flown to capture images of remote streams towards a fully remote streamflow observation procedure [*Fujita and Kunita*, 2011; *Tauro et al.*, 2015; *Detert and Weitbrecht*, 2015; *Perks et al.*, 2016].

Progress in image-based streamflow methodologies at the hydrological research level has not been paralleled by the implementation of similar prototypes in environmental monitoring practice. In our opinion, this can be attributed to the fact that technical software protocols for automated image processing are still missing; further, velocimetry algorithms tend to be sensitive to visibility conditions and the occurrence of floating materials on the stream surface. In particular, the accuracy of LSPIV, which is the most frequently adopted algorithm for streamflow observations, is dramatically reduced in case of dishomogeneous surface features, typical of low flow conditions, and adverse sunlight reflections. Conversely, for PTV to provide accurate (even if spatially sparse) velocity measurements, it is sufficient that a few particle-shaped tracers are captured in the field of view. The dependence of LSPIV on abundantly seeded surfaces and not excessive sunlight conditions hampers a systematic acquisition of LSPIV-based measurements.

Consistent with traditional PIV, LSPIV velocities are time-averaged values over the interval of observation. This approach is efficient in laboratory conditions, where the density and similarity of tracers as well as the presence of water patterns and reflections are fully controllable. Conversely, in the field, velocity vectors may be obtained by taking into account the displacement of a broad range of diverse items (such as, for instance, floating objects of varying shapes or water reflections and patterns, which may be stationary) transiting in the field of view [*Hauet et al.*, 2008a]. Therefore, underestimated velocities are frequently obtained, and attributing an uncertainty to such measurements is challenging. Comparisons of such time-averaged estimations to traditional point-wise measurements may also yield inaccuracies.

In this work, we comparatively examine LSPIV and PTV, and assess their suitability for streamflow measurements in the field. Both techniques present common aspects: they look for similarities between pairs of images and yield stream surface velocity distribution over a two-dimensional domain. However, LSPIV is a semi-Eulerian approach that estimates the velocity at image subregions, while PTV is a Lagrangian methodology that reconstructs the trajectory of individual particles transiting in the field of view. While several studies have focused on comparative analyses of PIV and PTV in laboratory conditions [*Nezu and Sanjou*, 2011; *Kähler et al.*, 2012], in this paper, the efficiency of the techniques is assessed in case of field measurements.

Based on our experience, we posit the hypothesis that the PTV approach is better suited than LSPIV for streamflow observations in natural settings. To provide unambiguous evidence for this fact, we evaluate the relative performance of the approaches to consistent experimental conditions by applying both methodologies on a dataset of 12 videos of a small stream. To offer a simple but sound testbed, we replicate LSPIV-favorable experimental settings by deploying tracers continuously and homogeneously on the stream surface. PTV is conducted by computing the trajectories of artificially seeded tracers and then filtering realistic paths to estimate velocities. In case both approaches give similar results, an additional test based on the analysis of a moderate flood in a larger scale riverine ecosystem, where naturally occurring debris serves as tracers, would help to identify the best approach. On the other hand, if LSPIV performance in favorable tests is poor as compared to PTV, then it would most probably fail in realistic conditions in a larger scale river.

2 Image-based methods for streamflow observations

2.1 Large Scale Particle Image Velocimetry (LSPIV)

LSPIV was developed based on conventional particle image velocimetry (PIV) to noninvasively measure the velocity field of large scale hydraulic and hydrological sys-

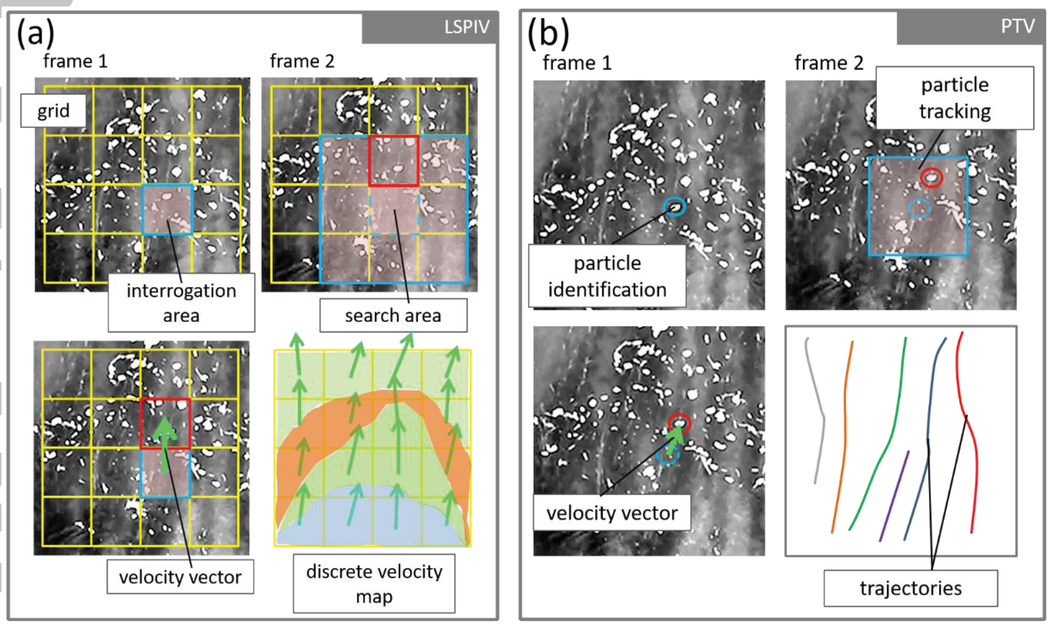

Figure 1. (a) Schematics of LSPIV: velocity is obtained by analyzing a number of consecutive frames with cross-correlation. Particle displacement is found from the highest similarity between the interrogation area in frame 1 and an area of consistent dimensions in the search area in frame 2. Velocity vectors are computed dividing the displacement by the time interval between consecutive frames. The procedure outputs a discrete velocity map. (b) Schematics of PTV: velocity is computed by analyzing a pair of frames. First, particles of selected shape and intensity are identified in frame 1, then the particles are tracked in frame 2. The approach aims at reconstructing particle trajectories in the field of view.

tems [*Fujita et al.*, 1997]. Standard PIV is a widely diffused quantitative flow visualization technique for fluid dynamics applications [*Adrian*, 1991, 2005], which entails the acquisition and analysis of digital images capturing seeded particles in a two-dimensional fluid domain [*Raffel et al.*, 2007]. Particle displacement in the plane is obtained by analyzing small regions (interrogation areas) of consecutive images through cross-correlation, Figure 1(a), (alternative algorithms have been presented in *Osorio-Cano et al.* [2013]; *Dobson et al.* [2014]; *Ran et al.* [2016]). Velocity vectors are then computed dividing the displacement by the time interval between consecutive images. Such velocities are assigned at an arbitrary point, that is, at the center of each interrogation area. Accurate estimations only rely on the selection of particles that appropriately follow the fluid flow [*Dramais et al.*, 2011; *Kantoush et al.*, 2011]. To this end, this approach is commonly adopted in case of high tracer concentration in the flow. In such conditions, cross-correlation is computed between image patterns rather than on individual tracer particles and, therefore, it is assumed that particles do not considerably change their relative position in the time interval between consecutive frames.

Different from standard PIV, LSPIV involves acquisition of a two-dimensional domain with low cost equipment [*Creutin et al.*, 2003; *Kim*, 2006; *Muste et al.*, 2008]. Commercial cameras are typically used in external sunlight conditions. To capture large views, cameras are frequently angled with respect to the water surface and, thus, image orthorectification and the acquisition of ground control points (GCPs) are mandatory. Sometimes, image enhancement is required to emphasize the appearance of tracers. In past studies, both naturally occurring floaters and artificially seeded objects have been used as tracers [*Bradley et al.*, 2002]. LSPIV has been extensively used for estimating river discharge and monitor flash floods [*Stumpf et al.*, 2016], small streams [*Gunawan et al.*, 2012], estuarine regions [*Bechle et al.*, 2012], and hydraulic structures [*Kantoush et al.*, 2011]. Further, due to inexpensive measurement apparatus, the technique has been applied to videos taken from Youtube [*LeBoursicaud et al.*, 2015] and recorded by citizen scientists [*LeCoz et al.*, 2016]. Among several factors, illumination and seeding conditions have been deemed as key controls of LSPIV accuracy. The identification of GCPs (and the consequent orthorectification process), seeding density, camera distance, and sampling time also introduce considerable uncertainty [*Kim et al.*, 2008].

In this study, we utilize PIVlab [*Thielicke and Stamhuis*, 2014], an open-source toolbox developed for the Matlab environment. The toolbox features region of interest and mask selection, basic image enhancement procedures, and cross-correlation in the spatial and frequency domain. Displacement peak location can be determined at the sub-pixel level with either a 2×3-point Gaussian fit or a $9-$point Gaussian fit [*Nobach and Honkanen*, 2005].

2.2 Particle Tracking Velocimetry (PTV)

PTV is a Lagrangian approach that determines randomly located velocity vectors based on the detection and tracking of individual particle tracers, Figure 1(b), [*Lloyd et al.*, 1995]. Application of PTV is designed for low seeding density flows and is documented for diverse environmental studies [*Moroni and Cushman*, 2001; *Uijttewaal et al.*, 2001; *Kimura et al.*, 2011; *Yossef and deVriend*, 2011]. Since velocities are estimated for individual particles and typically no assumptions are imposed on the relative position of neighbor particles, PTV has been widely applied to investigate unsteady flows [*Li et al.*, 2013]. Individual particle detection and tracking has been performed with a variety of algorithms, such as cross-correlation [*Lloyd et al.*, 1995], relaxation [*Wu and Pairman*, 1995], heuristics based on a priori knowledge of the flow [*Tang et al.*, 2008], and Voronoï tracking scheme [*Aleixo et al.*, 2011], among others.

In this study, we implement PTV following a modified command-line version of PTVLab [*Brevis et al.*, 2011], an open-source toolbox for Matlab. The toolbox allows for particle detection through either correlation with a Gaussian mask or dynamic threshold binarization [*Ohmi and Li*, 2000]. Particle tracking can be executed with cross-correlation, the iterative relaxation labeling technique, or a hybrid of the two approaches.

2.3 Comparison of the methodologies

	LSPIV	**PTV**
Setup	Remote installation based on inexpensive cameras. Cameras are either angled or orthogonal to water surface. Lasers can be used for remote image calibration.	Remote installation based on inexpensive cameras. Cameras are either angled or orthogonal to water surface. Lasers can be used for remote image calibration.

Surface appearance	Needs continuously and densely seeded surfaces. Potentially applicable with naturally-occurring floaters or patterns	Needs highly-defined particle-shaped floaters.
Algorithm	Cross-correlation between interrogation and search areas of frame pairs. Velocity vectors are arbitrarily assigned at the center of interrogation areas.	Identification and tracking of objects of a priori known shape and intensity. Velocity vectors are randomly located in the field of view.
	Outputs 2D surface velocity field at discrete spatial resolution.	Outputs tracers' trajectories and interpolated maps of 2D surface velocity field.
	Tracers within interrogation windows are assumed not to change their relative position between frame pairs.	Works well with unsteady flows.
	Requires several tracers per interrogation area.	Works with poorly seeded surfaces.
	Min. 2 input parameters in PIVLab.	Min. 6 input parameters in PTVLab.
	Dimensions of interrogation and search areas adjusted based on tracer dimension and velocity.	Tracer dimensions should be smaller than the frame-by-frame displacement, since the algorithm must follow the tracers' motion.
Controls	Tracers should be homogeneously distributed in the field of view during the entire analyzed image sequence.	Few tracers are allowed.

	Negatively impacted by sunlight reflections. Usually results in lower velocity estimations.	Negatively impacted by sunlight reflections. Trajectory-based filtering can help.

Table 1: Comparison of LSPIV and PTV working principle, requirements, and controls. Comparison is based on PIVLab and PTVLab implementations for LSPIV and PTV, respectively.

Image-based techniques present remarkable advantages with respect to traditional and point-wise instrumentation. In fact, they afford measurements of complex two-dimensional flow fields noninvasively and with relatively inexpensive equipment. Neither LSPIV nor PTV require a priori knowledge or assumptions on flow direction.

LSPIV is usually preferred to alternative image-based approaches since it should work with image patterns rather than with individual tracers. Therefore, it can be adopted with naturally occurring floaters of any shape or exploiting small fluctuation waves and heterogeneity of water color [*Tsubaki et al.*, 2011]. Generally, a priori knowledge of the shape and intensity of tracers is not requested; however, the dimension and frame-by-frame displacement of the patterns should be known to inform the selection of interrogation and search areas. On the other hand, PTV requires the presence of highly resolved tracers (whose shape should be known), which are most frequently manually added. For such reasons, PTV has been more widely adopted in laboratory studies rather than outdoors. Table 1 comparatively presents the working principle, requirements, and controls for LSPIV and PTV. Comparison is based on PIVLab and PTVLab implementations for LSPIV and PTV, respectively.

Several LSPIV studies consistently document the dependence of the technique on the presence, distribution, and brightness of tracers [*Kim*, 2006; *Muste et al.*, 2011]. Both high seeding density and diffused illumination conditions should be sought to lead to accurate velocity estimations [*Hauet et al.*, 2008b]. Ideal conditions are achieved when several particle tracers are found in each interrogation window. Based on numerous experimental studies in diverse environmental conditions, such high seeding densities can be rarely encountered in natural environments [*Muste et al.*, 2004; *Yu et al.*, 2015] (see also Figure 2). During floods, floating material tends to cluster in large scale objects; even if material is artificially seeded, particles agglomerate and are rarely evenly distributed across the entire

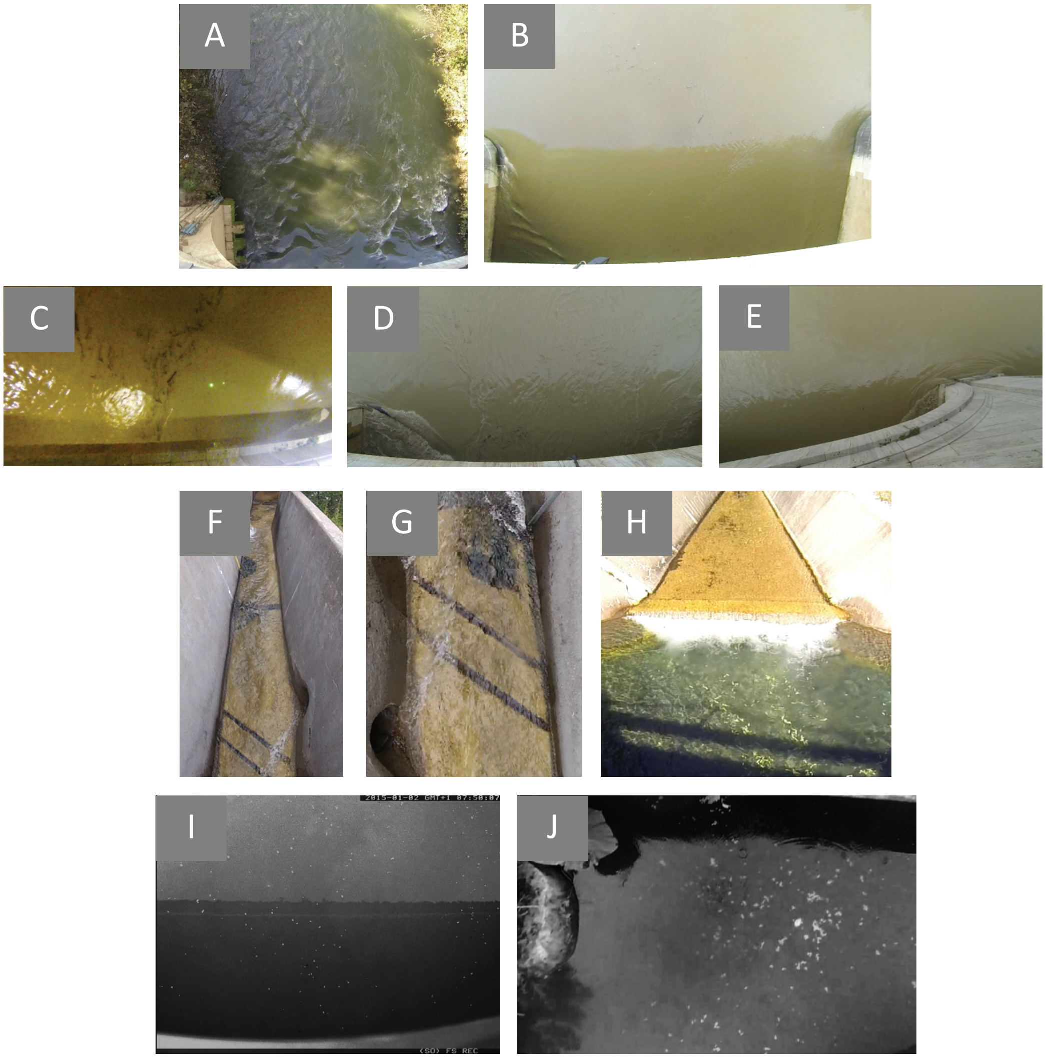

Figure 2. Appearance of the water surface in diverse LSPIV studies. Images (A) and (B) are taken from [*Tauro et al.*, 2014b]; (C), (D), and (E) from [*Tauro et al.*, 2016c]; (F) from [*Tauro et al.*, 2016d]; (G) and (H) from [*Tauro et al.*, 2016b]; (I) from [*Tauro et al.*, 2016a]; and (J) from [*Tauro et al.*, 2015]. LSPIV consistently resulted in underestimated velocities in these experimental conditions.

field of view [*Lewis and Rhoads*, 2015]. Hence, in outdoor natural environments, LSPIV is usually applied to analyze frames of rather extended areas captured at not excessively high definition [*Fujita and Kunita*, 2011; *Hauet et al.*, 2009; *Jodeau et al.*, 2008; *LeCoz et al.*, 2010]. Such applications allow for quickly capturing the large scale behavior of the flow but do not lead to spatially-refined results. If smaller areas are captured, the probability of finding several particle tracers per interrogation window sensibly decreases, and estimated velocities are unrealistically low [*Tauro et al.*, 2014b, 2016b,c,a].

Further difficulties related to practical LSPIV implementation are attributable to: i) image orthorectification, which produces less accurate and defined images; ii) acquisition of GCPs, which prevents application of the technique in difficult-to-access environment or requires post-event surveys; and iii) illumination conditions, such as glare, which add considerable noise and are difficult to correct for during post-processing [*Hauet et al.*, 2008b; *Lewis and Rhoads*, 2015]. While image orthorectification and the acquisition of GCPs have been circumvented by proposing alternative experimental setups and the use of lasers [*Tauro et al.*, 2014b], sunlight reflections still hinder the extraction of accurate LSPIV-based velocities. Finally, LSPIV is sensitive to image pre- and post-processing [*Lewis and Rhoads*, 2015], which are in turn determined based on the user's experience. In our opinion, this strong dependence of LSPIV on experimental settings and on the user's expertise limits its diffusion in environmental monitoring practice. LSPIV-based velocities are commonly computed by time-averaging frame-by-frame estimations. In fact, longer observations ensure higher probability of finding tracers in interrogation areas. The selection of the measurement duration depends on the specific experimental conditions and is determined on a case-by-case basis. Further, the longer the observation interval, the higher the probability that sparsely seeded regions in any given interrogation area will lead to a lower mean. Therefore, assigning uncertainty to LSPIV estimations and comparing LSPIV-based velocities to point-wise measurements is complex.

PTV may partially mitigate such criticalities. Technological advancements in optical equipment and electronics have allowed commercially-available low-cost cameras for high resolution capabilities and inexpensive equipment for extensive image storage and processing. Therefore, capturing small tracers (that is, imaging objects a few centimeters in diameter from up to 20 meters) at a sufficiently high resolution should not be a limitation for standard commercial cameras. Further, several studies demonstrate that PTV is less affected by illumination conditions [*Tauro et al.*, 2016a; *Tauro and Salvatori*, In press], which typically hamper accurate LSPIV-based estimations. Finally, PTV can be used to reconstruct individual tracers' flowpaths. The identification of specific objects in the field of view is expected to alleviate velocity underestimations and to provide a tangible basis to assess measurement accuracy. However, PTV may be limited in the detection of irregularly-shaped objects and provide more sparsely-refined measurements than LSPIV. Thus, PTV has not been used as successfully as LSPIV in large-scale environments to characterize flow structures that are coherent or semi-coherent.

2.4 Trajectory-based filtering for PTV

To improve velocity estimation with PTV, we slightly modified the implemented command-line version of PTVLab to store the coordinates of identified tracers in each image for each recognized path. Trajectories were then filtered by post-processing tracer coordinates associated to specific paths. Similar approaches have already been applied to PTV studies in the literature. For instance, in *Hassan and Canaan* [1991], a PTV "track" method is proposed, whereby tracer trajectories are retained for velocity estimation if they exhibit minimum variance of length and angle of travel between successive frames, and if the detected particles proceed for a minimum length in the field of view. In our method, it was assumed that the camera field of view was directed with its width along the river cross-section and that the height of the field of view was orthogonal to the cross-section, Figure 3. We supposed that particles tracked along individual paths moved forward (that is, their trajectories should be fairly orthogonal to the river cross-section). These simple assumptions are consistent with previous work by *Hassan and Canaan* [1991], and do not generate "false" vectors that may bias results. In previous studies [*Tauro and Grimaldi*, 2017], we verified that trajectories slanted with respect to the cross-section are often obtained in case of ambiguities (such as close-by particles that form agglomerates and separate while proceeding in the field of view). Therefore, when two successive frames (that is, frames k and $k-1$) were considered, tracer position vectors $\vec{X}_k$ and $\vec{X}_{k-1}$ should satisfy the following condition:

$$\arctan\left[\frac{(\vec{X}_k - \vec{X}_{k-1}) \cdot \boldsymbol{j}}{(\vec{X}_k - \vec{X}_{k-1}) \cdot \boldsymbol{i}}\right] > \frac{\pi}{4} \tag{1}$$

whereby, $\boldsymbol{j}$ and $\boldsymbol{i}$ were unit vectors in the directions orthogonal and parallel to the river cross-section, respectively. If tracer coordinates satisfied Eq. (1), trajectories were further selected based on their length and slant. Namely, we only retained trajectories slanting up to 80° from the river cross-section and that extended for at least 20% of the height of the field of view (H). The first condition was imposed through

$$\arctan\left[\frac{(\vec{X}_{\text{end}} - \vec{X}_{\text{start}}) \cdot \boldsymbol{j}}{(\vec{X}_{\text{end}} - \vec{X}_{\text{start}}) \cdot \boldsymbol{i}}\right] > \frac{4}{9}\pi \tag{2}$$

whereby $\vec{X}_{\text{end}}$ and $\vec{X}_{\text{start}}$ indicated the tracer position vectors in the final and first images of the trajectory, respectively. The length of the trajectory was validated through

$$\|\vec{X}_{\text{end}} - \vec{X}_{\text{start}}\| > \frac{1}{5}\text{H}. \tag{3}$$

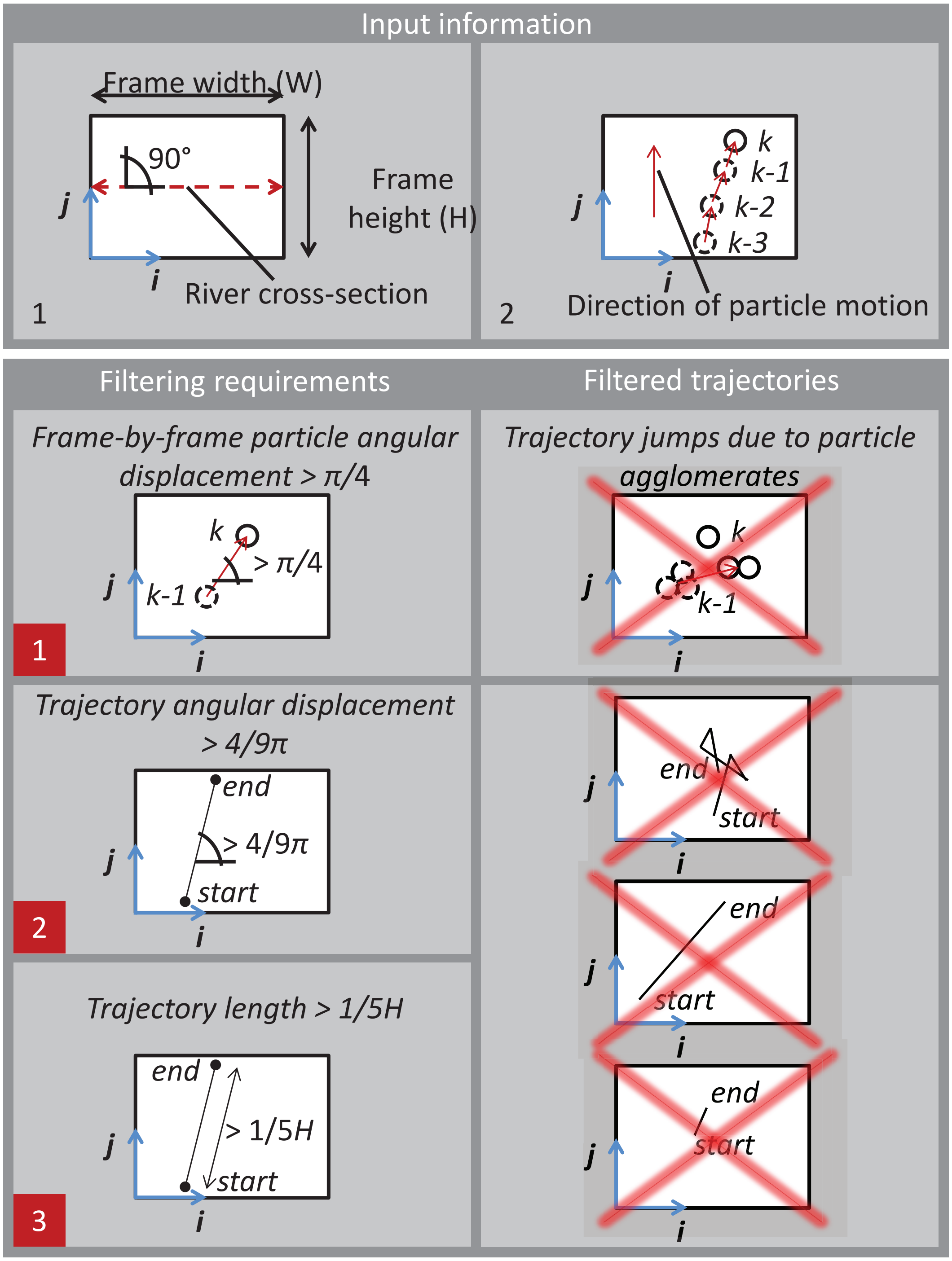

Figure 3. Diagram of the input information and requirements of the trajectory-based filtering procedure.

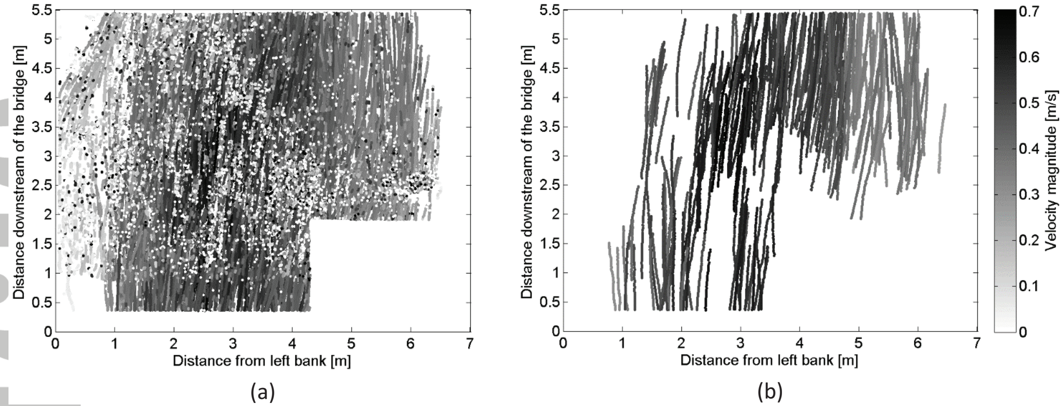

Figure 4. Application of the trajectory-based filtering methodology. In (a), all trajectories identified through the command-line version of PTVLab are displayed. In (b), filtered trajectories are reported.

Streamflow velocity for each trajectory (V) was then determined as

$$V = \frac{\|\vec{X}_{\text{end}} - \vec{X}_{\text{start}}\|}{\Delta t} \tag{4}$$

where Δt was the time interval between the final and first images of the trajectory.

In Figure 4, we report a sample application of the illustrated methodology. In Figure 4(a), all trajectories identified through the command-line version of PTVLab are displayed. Figure 4(b) only illustrates trajectories that satisfied our constraints and were utilized to estimate streamflow velocity. As illustrated, the methodology ensures that only trajectories parallel to the main flow direction are retained for velocity estimation.

3 Experimental analysis

In this work, we evaluated the relative performance of LSPIV and trajectory-based filtering PTV by analyzing a data set of 12 image sequences captured on a small scale stream. Based on our previous experience on the sensitivity of the algorithm to the presence of tracers, LSPIV is less adequate for streamflow observations in natural settings than PTV. Such hypothesis was tested by replicating LSPIV-favorable experimental conditions. Specifically, we devoted special care to continuously deploy abundant quantities of evenly distributed tracers on the stream water surface for the entire duration of the acquisitions. While PTV is less favored by densely seeded images and computational time considerably increases, previous research supported the robustness of this technique in challenging settings [*Tauro and Salvatori*, In press]. If LSPIV performance was poor in such favor-

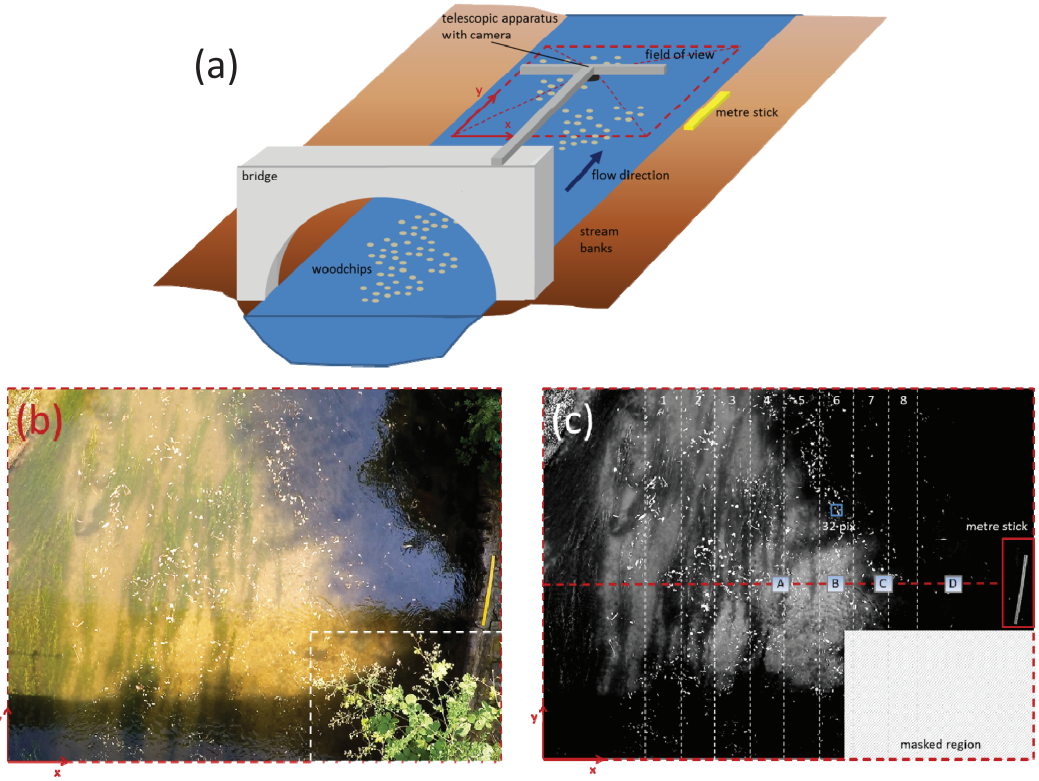

Figure 5. (a) Sketch of the experimental setup and apparatus on the Brenta River; (b) RGB experimental image; and (c) representative processed image depicting the field of view, locations of the current meter measurements (A to D), and vertical regions used for comparing velocities obtained with LSPIV and PTV

.

able settings, then the algorithm would have most probably failed in realistic conditions in a larger scale river. Therefore, both algorithms have been further tested in realistic conditions, that is, by analyzing images recorded during a moderate flood in a larger scale riverine ecosystem.

3.1 Brenta River

3.1.1 Experimental site and materials

A set of experiments was performed on the Brenta River at the bridge "Ponte Zaccon", Trento, Italy, (46°02′20.8122″ North Latitude, 11°24′37.3349″ East Longitude, 464.38 elevation in the WGS84 coordinate system) on June 10th, 2015. Therein, a monitoring station that hosts an ultrasonic water level meter is run and managed by Provincia Autonoma di Trento (PAT). The station monitors the upper basin of the Brenta River (171.9 km^2), and it features a 10.1 m-wide rectangular cross-section. During the experiment, a water level of approximately 0.41 m was recorded at the nearby monitoring station. The river banks are steep and reinforced in stone blocks. A few meters upstream of the monitoring station, river banks are relatively accessible for on site testing and observations. The bridge parapet is constructed from iron profiles, which allow to easily install experimental instrumentation. At the monitoring station, the river bed presents green filamentous algae, pebbles, and wood detritus, that contribute to decrease the visibility of floating objects.

According to data collected by PAT in 2009-2010, the average stream discharge peaks in late spring (2.56 m^3/s in June), is minimum in summer (1.48 m^3/s in August), and increases in winter (2.19 m^3/s in February). Throughout the year, the water level ranges from a minimum of 0.39 m to 0.47 m. Notably, the study site is only equipped with an ultrasonic water level meter. Rating curve as well as wind and temperature data are not available at the stream reach.

In our design, experiments were conducted by continuously deploying woodchips from the upstream side of the bridge. To maximize the chances of homogeneous distribution of floating material in the field of view, six equidistant operators launched material during video acquisition. The portable telescopic apparatus developed in [*Tauro et al.*, 2014b] was installed on the downstream side of the bridge, Figure 5(a). The apparatus featured a GoPro Hero 4 Black edition camera oriented with its axis orthogonal to the water surface. The system also hosted two green laser modules for remote image calibration; however, due to strong light intensity, lasers were not clearly visible in images. A metre stick was placed on the right-side stream bank at the same level of the water surface for calibration purposes, Figure 5(b).

To provide a reference velocity measurement, an OTT Hydromet C2 current meter was used to capture velocities right below the water surface along a cross-section parallel to the bridge. Measurements were conducted at a few (3 cm) centimeters below the water surface at four locations along the stream cross-section up to 3.5 m from the right-side river bank. Additional acquisitions towards the left-side river bank were challenging due to the presence of vegetation. Measurements were conducted in the time mode: the measuring time required was set to 10 s, the propeller revolutions were automatically counted

Table 2. Average benchmark velocities ($\overline{v}_\mathrm{b}$) and standard deviations (σ_b) measured with the current meter at locations illustrated in Figure 5(c).

	A	B	C	D
$\overline{v}_\mathrm{b}$[m/s]	0.46	0.45	0.31	0.32
σ_b[m/s]	0.04	0.03	0.02	0.02

during the measuring time and water velocity was instantly derived from the speed in rotations per second through the instrument calibration equation. Figure 5(c) depicts the measurement locations: measures were taken at 1 m, 2 m, 2.7 m, and 3.5 m from the right-side stream bank (locations D to A in Figure 5(c)). Twelve replicates were performed at each location; average velocities ($\overline{v}_\mathrm{b}$) and standard deviations (σ_b) are reported in Table 2. On average, flow velocity close to the stream surface was estimated to be slightly less than 0.4 m/s.

3.1.2 Image processing

A Full HD (1920 × 1080 pixels) RGB video captured a stream reach of $9.5 \times 5.3\,\mathrm{m}^2$ for 4:11 minutes at 50 Hz. Such a high acquisition frequency was initially selected to guarantee a sufficiently large number of images to depict the transit of floating objects in the field of view. Image fisheye distortion was removed using the open-source software GoPro Studio. Out of the original video, 12 video sequences of 20 s each were extracted. The selection of such observation intervals were constrained by practical difficulties in continuously and homogeneously seeding the river for longer times. Similar short intervals were set in previous LSPIV studies [*Tauro et al.*, 2014b]. Given the moderate stream flow velocity, image sequences were subsampled at 25 Hz and river banks were trimmed. Analyzed images were 1430 × 1080 pixels in resolution (corresponding to a field of view of $7.1 \times 5.3\,\mathrm{m}^2$), Figure 5(b). The bottom right corner of the images displayed vegetation leaning from the bridge and, to prevent disturbances in velocity estimation due to vegetation motion, an area of 552 × 375 pixels was masked with a black patch. Original RGB images were converted to grayscale intensity by eliminating hue and saturation information and retaining the luminance. To emphasize lighter particles against a dark background, images were gamma corrected to darken midtones [*Forsyth and Ponce*, 2011]. On average, particles were 10 pixels in diameter, and moved by 6 pixels between consecutive frames.

3.1.3 LSPIV analysis on the Brenta River

LSPIV was implemented on experimental images using PIVlab. In accordance with *Keane and Adrian* [1990], to ensure a minimum displacement of the particle tracers of at least 8 pixels between consecutive images (that is, a fourth of the interrogation window size), frame sequences were again subsampled to 12.5 Hz; therefore, each LSPIV sequence comprised a total of 250 frames. To maximize information, images were analyzed adopting the sequencing style 1-2, 2-3, which yielded 249 velocity fields. Images were preprocessed to enhance the appearance of tracers with respect to the background by applying a Gaussian high pass filter (filter size set to 15 pixels) that boosts particle intensity in case of inhomogeneous lighting. Further, frames were denoised through Wiener filtering (filter size set to 10 pixels) [*Lim*, 1990].

A preliminary parametric analysis was executed to identify optimal LSPIV settings. Cross-correlation was evaluated using a standard direct cross-correlation (DCC) and setting the interrogation area to 32×32 pixels, and the grid size to 16×16 pixels, respectively, see a representative interrogation window in Figure 5(c). Such values were selected upon a preliminary parametric analysis. DCC was chosen since, according to *Thielicke and Stamhuis* [2014], it shows more accurate results than discrete Fourier transform. Also, interrogation window iteration and window deformation were not considered since, as stated in *Scarano and Riethmuller* [2000], these techniques were mainly introduced to extend the velocity and velocity gradient dynamic range, which is not relevant in the presented applications in low velocity environmental flows. Apart from areas without tracers, a number of five to eight particles were depicted in interrogation windows, whereby each particle ranged in diameter within 10 to 15 pixels. The 2×3-point Gaussian fit was used as sub-pixel displacement peak estimator. Image calibration was performed by estimating the pixel dimensions of the metre stick. The time interval between consecutive frames was a priori known. Data were validated by applying velocity upper and lower thresholds. Thresholds were semi automatically determined as $\bar{u} \pm n * \sigma_{\mathrm{u}}$, with $\bar{u}$ the mean velocity for each analyzed frame pair, σ_{u} its standard deviation, and n set to 3. The velocity field for each frame sequence was obtained by averaging in time the velocity field computed for each frame pair.

3.1.4 PTV analysis on the Brenta River

PTV was performed using a modified version of PTVLab, which allows for serial analysis of massive image datasets through a command-line interface [*Tauro and Salvatori*, In press]. Particle detection entails image binarization via thresholding and cross-correlation with a symmetric Gaussian kernel thus, the image intensity threshold, the standard deviation of the Gaussian distribution, and the correlation cutoff threshold need to be defined. Based on preliminary parametric analyses, the intensity grayscale level was set to 130, the standard deviation to 12 pixels, and the correlation threshold to 0.5. Particle tracking was implemented using cross-correlation by interrogation area. The tool requires the size of the square interrogation area, the cross-correlation cutoff threshold, and the similarity percentage among neighbor particles to be defined as inputs. Specifically, the interrogation area was set to 20 pixels, the cross-correlation threshold to 0.4, and the neighbor similarity percentage to 20%. Once analyzed, the ID of each tracked particle along with its pixel coordinates were saved as an ascii file and processed with the trajectory-based algorithm presented in Section 2.4.

3.1.5 Velocity data comparison

To offer a comparison among LSPIV, PTV, and benchmark measurements taken with the current meter, "lumped" values were obtained from image-based spatially-distributed LSPIV and PTV velocities. To this end, the field of view was divided into eight vertical regions (see the dashed lines in Figure 5(c)). Since video sequences were rather short, statistically stationary conditions could be assumed in vertical regions during the observation interval. The average velocity along each region was computed from both LSPIV and PTV acquisitions and then compared to the benchmark measurements. More specifically, the eight vertical regions were selected to be homogeneous in width and to exclude the areas close to the river banks, where less tracers were observed.

With regards to LSPIV, surface flow velocity maps were developed for each of the 12 image sequences. For each sequence, a time-averaged LSPIV map was obtained by averaging over the 249 outputs of the cross-correlation. We overlayed the vertical regions to time-averaged maps and computed the average velocity and standard deviation pertaining to each region. The average velocity and standard deviation were computed based on either 396 or 462 elements (each vertical region comprised either 6 or 7 columns of the PIV

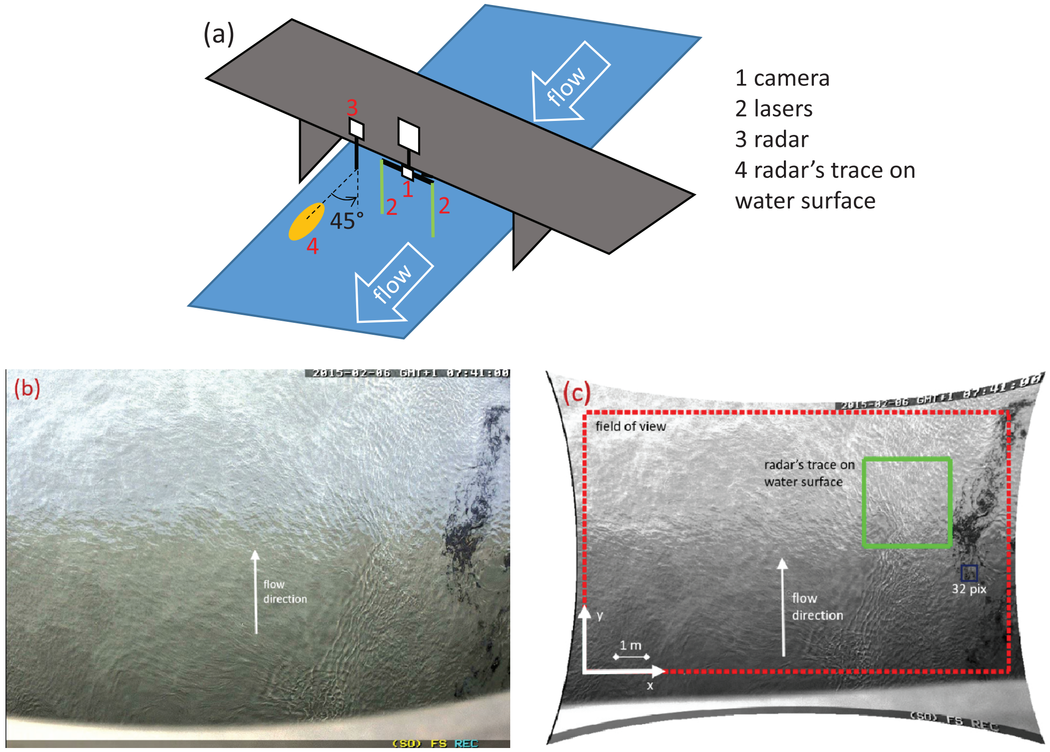

Figure 6. (a) Sketch of the experimental setup on the Tiber River; (b) RGB experimental image; and (c) representative processed image depicting the field of view and radar's trace on the water surface. The blue box indicates the dimensions of the interrogation area.

grid). In case of PTV data, the number of trajectories laying in the vertical regions ranged from a minimum of 5 in region 8 (left-side stream bank) to a maximum of 56 in region 6. "Lumped" average velocities and standard deviations in the vertical regions were obtained by averaging over the values obtained with Equation 4 for each trajectory.

3.2 Tiber River: a proof-of-concept during a flood event

3.2.1 Experimental site and materials

Flood images were captured in the Tiber River on February 6th, 2015, through the gauge-cam station recently installed on the Tiber River underneath the bridge "Ponte del Foro Italico" in the city of Rome, Italy [*Tauro et al.*, 2016a; *Tauro and Salvatori*, In press], Figure 6(a). The gauge-cam station enables the acquisition of one-minute long videos every ten minutes through a Mobotix FlexMount S15 weatherproof internet protocol camera. The camera comprises two optical modules with independent sensors and lenses. The right-side L25 lens (82° angle of view and 4 mm focal length) captures a large area of the river surface, whereas the left-side L76 lens (27° angle of view and 12 mm focal length) enables finer observations in the center of the L25 sensor field of view. Both optical modules are placed with their optical axis perpendicular to the water surface to minimize distortions, thus eliminating the requirement of orthorectification, assuming negligible slope. Obviously, the dimensions of the field of view captured by the camera vary in accordance with the water level (and, therefore, with the distance of the camera from the water surface). The Tiber River bed slope in proximity of the station site is quite regular and mild, therefore, the water surface depicted in the camera field of view can be assumed horizontal. The gauge-cam station features a system of two < 20 mW green (532 nm wavelength) lasers installed at 50 cm on both sides of the camera. The lasers are activated for 20 s at the beginning of each video, and generate highly visible reference points located 1 m apart on the water surface. This laser system enables image calibration (that is, assigning a metric dimension to image pixels) without the use of ground control points. The MOBOTIX S15 camera enables maximum frame rates of 30 Hz (that is, 15 Hz per each optical module) either when significant motion occurs in the field of view [*MOBOTIX*, 2017] or when illumination intensity is high [*Tauro et al.*, 2016a]. Practically, the frame acquisition frequency of the gauge-cam station is automatically adjusted based on external illumination conditions and, thus, varies for each captured clip. Further, each one-minute long video is saved as numerous highly-compressed and reduced-size clip files (where the number of clips depends on the size of the video and, in turn, on the acquisition frequency).

We studied a one-minute video captured during the flood peak at 7:40 a.m., Figure 7. At the time of the peak, the ULM 20 ultrasonic meter and RVM20 speed surface radar installed on the same bridge next to the gauge-cam station recorded a water level of 7.23 m and an average surface velocity of 2.33 m/s, respectively. During the flood, the transit of debris and vegetation was observable on the river surface as well as numerous water ripples, Figure 6(b). Generally, floating material tended to clump together to form objects on the order of 100×100 pixels. To facilitate the identification and tracking of such objects, we only analyzed images recorded with the L25 lens, which captured an area of $16.15 \times 12.11\,\mathrm{m}^2$.

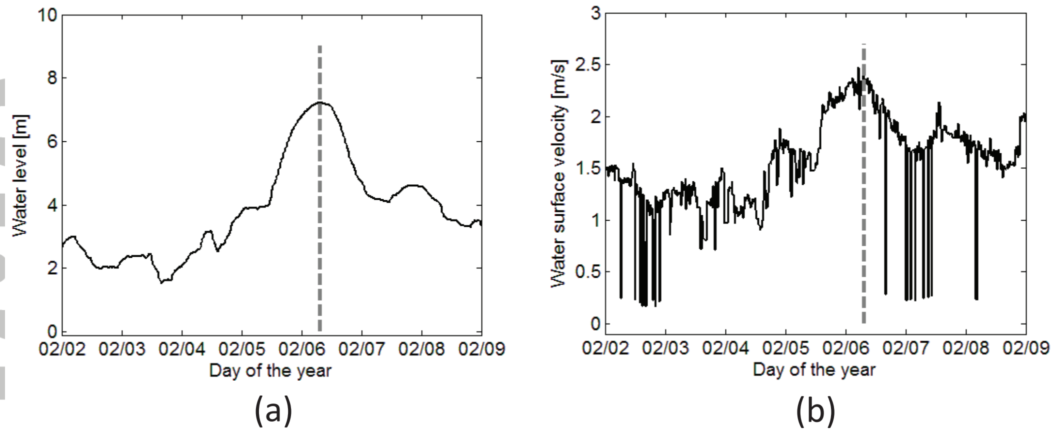

Figure 7. (a) Water levels and (b) radar velocities at "Ponte del Foro Italico", Rome, Italy. The dashed gray line indicates the time (7:40 a.m.) at which the selected video was captured during the flood peak on the 6th of February 2015. Water level and velocity data are recorded every 15 minutes.

3.2.2 Image processing

The selected video was saved as nine different clips whose duration and acquisition frequency ranged within 4 to 8 s and from 4 to 8.72 Hz, respectively. The analyzed sequence was obtained by decompressing each clip and the overall frequency was estimated to 6.95 Hz as a weighted average of each clip's frequency. Despite this relatively low frequency, the dimensions of the field of view enabled the application of LSPIV and PTV. Image resolution was set to 1024×768 pixels for both optical modules. Images of the flood on the Tiber river were affected by barrel distortion due to the wide-angle L25 lens. Fisheye distortion was removed using the Adobe Photoshop "Lens correction" filter.

3.2.3 LSPIV analysis on the Tiber River

Before LSPIV processing, images were trimmed to 865×530 pixels to remove highly distorted borders, see the dashed red area in Figure 6(c). The sequencing style 1-2, 2-3, was adopted, which yielded 409 velocity fields. Images were processed using cross-correlation through DCC and setting the interrogation area to 32×32 pixels and the grid size to 16×16 pixels, respectively. Such values were chosen based on a preliminary parametric analysis. A representative interrogation window is shown in Figure 6(c). The 2×3-point Gaussian fit was used as sub-pixel displacement peak estimator. Image calibration was performed by estimating the pixel distance between reference points illuminated by the lasers. The time interval between consecutive frames was a priori known from the overall acquisition frequency.

Similar to data on the Brenta River, data were validated by applying velocity upper and lower thresholds based on the value of the standard deviation (n set to 3). The velocity field for each frame sequence was obtained by averaging in time the velocity field computed for each frame pair.

3.2.4 PTV analysis on the Tiber River

Images were analyzed using the modified version of PTVLab and then trajectories were processed with the procedure in Section 2.4. Before processing, a region of interest was identified to exclude highly distorted image borders from the analysis. Particles were detected through correlation with a Gaussian mask of 12 pixels in diameter and 90 in maximum intensity. A correlation threshold of 0.5 was associated to potential particles. Particle tracking was implemented using cross-correlation and by setting similar parameters to Section 3.1.4.

4 Results and Discussion

4.1 Brenta River

Figure 8(a) displays a time averaged map obtained by analyzing LSPIV data for one image sequence. Vertical regions are illustrated through yellow vertical lines. As expected, surface velocity is higher (maximum velocity is equal to 0.53 m/s) in the center of the stream and decreases close to the stream banks. For the selected video, mean surface flow velocity is equal to 0.26 m/s and standard deviation to 0.14 m/s. In Figure 8(b), the signal-to-noise ratio (SNR) of the same representative video is illustrated. The parameter SNR is computed by dividing the mean value of each interrogation window by its standard deviation. Higher SNR values (darker pixels) are found in the center of the field of view, where a larger number of tracers transit. Also, higher accuracy is found in the southern horizontal region close to the bridge, where the bridge shadow leads to higher contrast of the tracers against the dark background (see also Figure 5(c)).

Representative maps of the PTV particle trajectories for one of the image sequences are displayed in Figure 9. In (a), the map illustrates all trajectories identified in PTVLab. Water reflections lead to abundant low velocity trajectories, depicted as lighter dots in Fig-

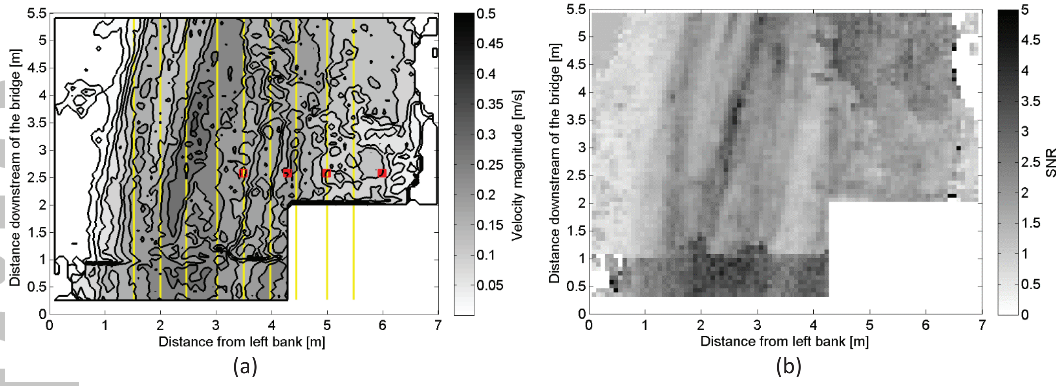

Figure 8. (a) Time averaged LSPIV map and (b) signal-to-noise ratio of a representative video captured on the Brenta River. In (a), yellow vertical lines illustrate vertical regions and red squares indicate the locations of the current meter measurements.

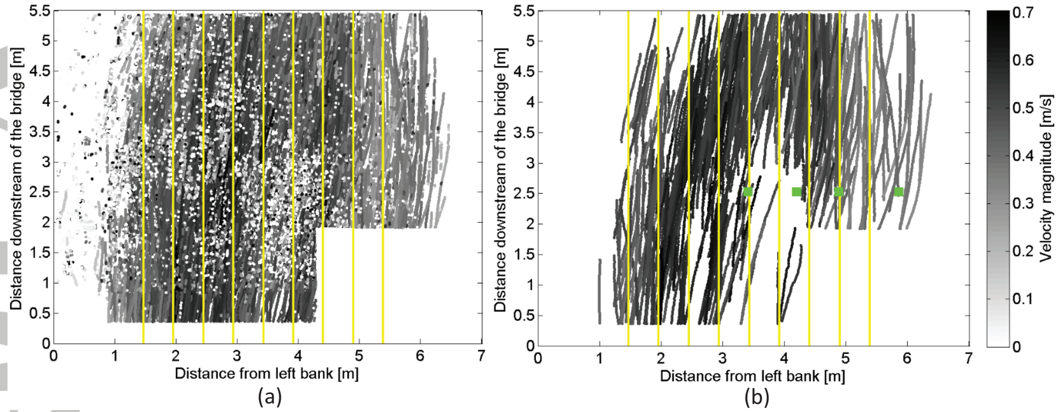

Figure 9. (a) Unfiltered and (b) filtered trajectories on the Brenta River. The colorbar indicates the velocity magnitude of each trajectory as obtained through Eq. 4. Yellow vertical lines indicate the vertical regions. In (b), the locations of benchmark current meter measurements are highlighted through green squares.

ure 9(a). This is due to the fact that many reflections are static and do not follow the flow. Conversely, in the right panel, the map reports trajectories retained after the filtering procedure. All trajectories pertain to actual floaters that transited in the field of view, thus guaranteeing reliable velocity estimation.

PTV and LSPIV data located in each of the vertical regions were averaged over the 12 replicates, and mean values and standard deviations computed. Average means and standard deviations over the replicates are reported in Figure 10(a). Therein, data points are surface flow velocity means, and standard deviations are represented as shaded regions. Both image-based approaches correctly capture the higher velocity at the center

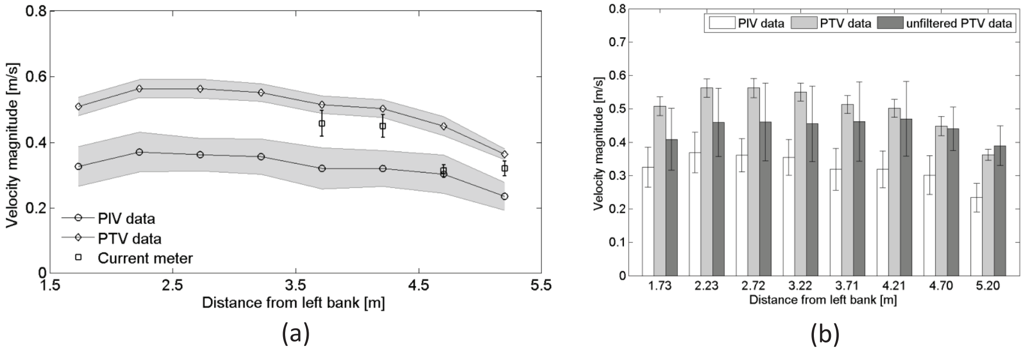

Figure 10. (a) Comparison between PTV and LSPIV data for experiments on the Brenta River. Values recorded with the current meter are also reported. Shaded regions indicate standard deviations. (b) Comparison between LSPIV, PTV, and unfiltered PTV data for experiments on the Brenta River.

of the stream cross-section. PTV data are generally higher than LSPIV estimations: PTV mean values are on the order of 0.5 m/s, whereas LSPIV means are on average equal to 0.3 m/s. Standard deviations are on the same order for both methods (on average equal to 0.05 m/s). In Figure 10(a), values computed from image-based methodologies in vertical regions 5 to 8 (see Figure 5(c)) are compared to measurements with the current meter (reported in Table 2). PTV average values are in close agreement with current meter measurements (PTV data are within 10.5% to 11.8% greater than current meter measurements) apart from values computed at 4.7 m from the left-side stream bank, whereby PTV data are 30.3% larger than the current meter value. This is probably due to the irregular stream bed or to the proximity of the propeller to the free surface. On the other hand, LSPIV data tend to underestimate surface flow velocity. It should further be noted that the current meter only provides a component of the actual velocity vector. Therefore, actual velocities are expected to be higher than current meter data. Analyzed through one-way analysis of variance (anova), image-based data and current meter measurements are not statistically different ($p = 0.22$ and $p = 0.09$ for PTV and LSPIV, respectively). However, tested with one-way anova, differences between PTV and LSPIV data are statistically significant ($p \ll 0.01$).

In Figure 10(b), we also compare means and standard deviations obtained with LSPIV, PTV, and unfiltered PTV. Unfiltered PTV data are directly obtained by processing the output from PTVLab, that is, without applying the trajectory-based filtering procedure. Generally, unfiltered PTV mean values are higher than LSPIV but lower than filtered PTV

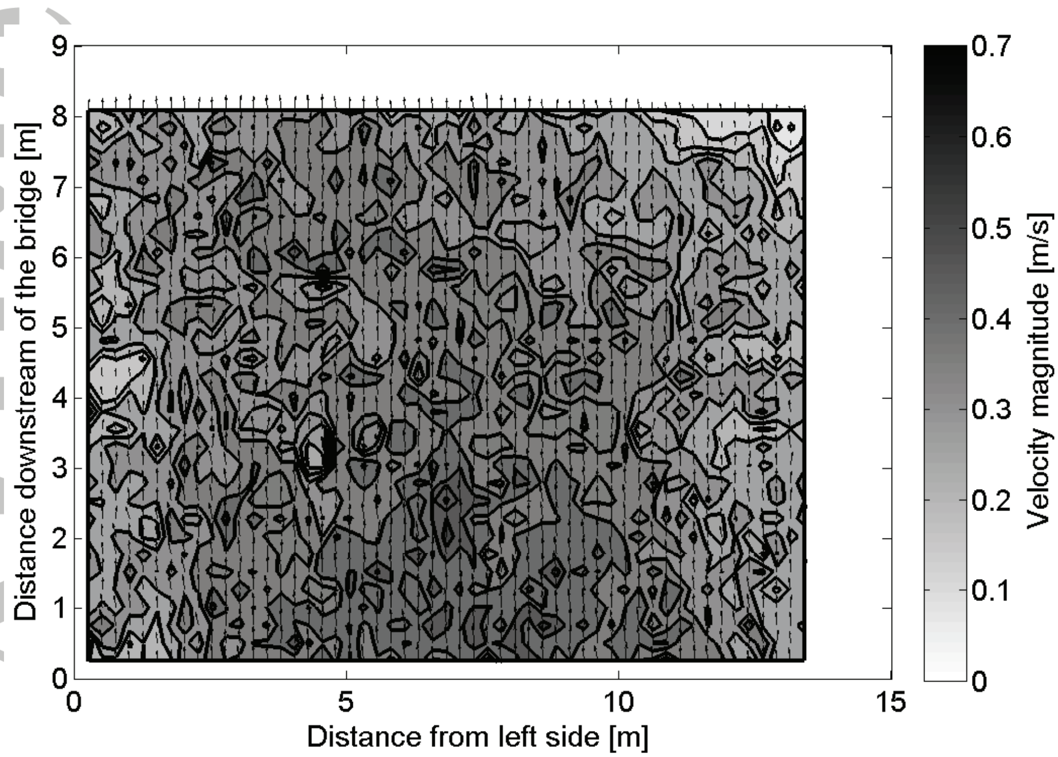

Figure 11. Time averaged LSPIV map of the Tiber River.

data. Standard deviations from unfiltered PTV data are much higher than the alternative algorithms (on average, on the order of $0.2\,\mathrm{m/s}$). This is due to the fact that all trajectories are retained in the computation and that water reflections are tracked by the algorithm even if they do not follow the water flow.

Although experimental settings were ideal for LSPIV analysis (the flow was stationary, artificial floaters were continuously and homogeneously dispersed onto the stream surface), the algorithm consistently underestimated flow velocity. This is in agreement with previous experimental findings [*Tauro et al.*, 2014b, 2016c] in natural streams, where naturally occurring objects were used as tracers. We attribute such inaccuracy to the tendency of tracers to agglomerate into clustered objects on the river surface. Due to tracer clustering, large regions of the field of view lack surface features and, therefore, lead to low velocities.

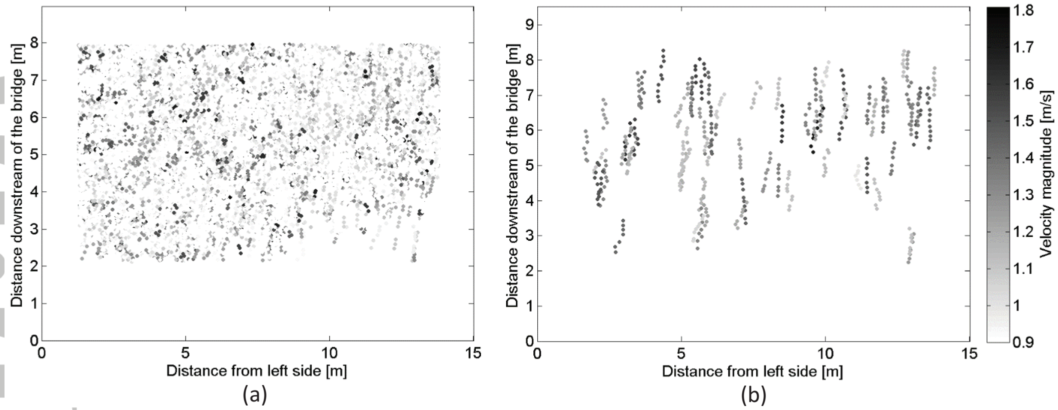

Figure 12. (a) Unfiltered and (b) filtered trajectories on the Tiber River. The colorbar indicates the velocity magnitude of each trajectory as obtained through Eq. 4.

4.2 Tiber River

Figure 11 depicts the time averaged surface flow velocity LSPIV map for the flood event on the Tiber River. Velocities are higher in the center of the field of view but scarcely represent actual flow conditions. In particular, mean velocity over the field of view is equal to 0.39 m/s and the standard deviation to 0.07 m/s. The maximum flow velocity computed in the field of view is 0.58 m/s, which is well below radar's measurements (> 2 m/s).

In Figure 12, a map of PTV particle trajectories after trajectory-based filtering is displayed. Even if few trajectories are retained with the filtering procedure (only 68 trajectories were retained out of more than 19000), they are correctly directed along the stream flow direction.

The appearance of floating objects during the flood event did not facilitate application of LSPIV nor PTV. With regards to LSPIV, time averaged surface flow velocity maps tended to be much less noisy and the mean velocity got closer to PTV estimations by increasing the interrogation window size (for instance, setting it to 64 pixels × 64 pixels or 128 pixels × 128 pixels). However, the respective velocity metrics highlighted some inconsistencies: maximum values were greater than the radar value, standard deviations were quite high, and, in some cases, velocity vectors were opposite to the flow direction. This can be explained with the fact that, even if the video was captured during a moderate flood, the field of view was not fully covered with tracers and less than 5 to 10 particles were present in each interrogation window. PTV was negatively affected by the irregular shape of the tracers, and, therefore, led to few meaningful trajectories. Most of the trajectories were irregular and short and, even upon trajectory-based filtering, surface flow velocity was estimated to be equal to 1.4 m/s, which is well below 2.33 m/s, as estimated by the radar.

Besides the irregular shape of tracers, inaccurate tracking was also due to the occurrence of numerous water reflections (see the lighter dots in Figure 12), which are sometimes identified as particles, and to inhomogeneous lighting conditions (the bridge shadow divides the field of view in an upper brighter region and in a darker lower area).

4.3 Limitations and possible ameliorations of image-based methods

Based on our experimental findings and previous research activities, LSPIV is not ideal to study the surface flow velocity field of natural water bodies. Specifically, the LSPIV algorithm leads to velocity vectors that are arbitrarily located at the center of a user-defined grid, and are time-averaged values over the interval of observation. This latter fact results in accurate estimations in laboratory controlled conditions, where users continuously and homogeneously (and probably in a much smaller field of view) deploy tracers. In the field, LSPIV-based velocity vectors are instead obtained by averaging the displacements of many different items (such as, for instance, floaters, water patterns, water reflections) transiting in the interrogation window for the entire duration of the observation interval. Since the density and similarity of tracers as well as the presence of water patterns and reflections in interrogation windows are not fully controllable in field conditions, attributing an uncertainty to such LSPIV-based velocity estimates is difficult.

In our tests, even if experimental conditions were carefully designed to facilitate LSPIV application, flow velocities were consistently underestimated due to tracer clustering and irregular lighting conditions. Both issues affected all experimental campaigns and are impossible to mitigate unless sophisticated equipment is used or rather small areas are artificially seeded. Analyzed with alternative LSPIV algorithms (that is, MatPiv [*Sveen*, 2004] and FUDAA [*Hauet et al.*, 2017]), similar velocity maps were obtained. Specifically, average velocities for one video captured on the Brenta River was found equal to 0.19 and 0.11 m/s for MatPiv and FUDAA, respectively. To further assay the effect of LSPIV velocity vector post-processing, the upper and lower thresholds validation technique (see Section 3.1.3) was compared to a median filter with 3×3 pixels size and to the local median filter by [*Westerweel and Scarano*, 2005] for a representative video captured on the Brenta River. Consistent results in terms of mean velocity and standard deviation were found for the different approaches. Specifically, the time averaged velocities of the obtained maps were equal to 0.26, 0.41, and 0.30 m/s, for the upper and lower thresholds, the median, and the local median filters, respectively. Post-processed with different approaches, LSPIV data still resulted underestimated as compared to PTV and the current meter measurements.

Since our fields of view were significantly smaller than several LSPIV studies [*Creutin et al.*, 2003; *Dramais et al.*, 2011], we suggest that such a technique is adopted to provide approximate estimations of the flow velocity field in large scale environments (on the order of hundreds or thousands of squared meters). In fact, by providing velocity estimates at the spatial resolution of the interrogation window, LSPIV data tend to be smoothed and underestimated as compared to PTV. Alternatively, LSPIV could be applicable in small yet highly seeded stream reaches. For instance, in case of sufficiently seeded surfaces, good LSPIV estimates have been obtained in vegetated environments by *Creëlle et al.* [2016].

In our experiments, improved description of the flow field has been achieved with PTV. In fact, PTV is based on the identification and tracking of recognizable physical objects. By imposing a few constraints on PTV-based trajectories (that is, if the river reach is rectilinear, trajectories should also be rectilinear and they should cover at least a fifth of the field of view), velocity estimations are closer to benchmark values. In the presence of water reflections, trajectory-based filtered PTV led to more reliable velocity estimations than LSPIV. In the case of experiments on the Brenta River, velocities were closer to current meter measurements. With regards to the Tiber River, even if a majority of the trajectories were short and irregular (probably due to irregularly shaped tracers), velocity estimation was significantly larger than LSPIV.

Processing images with PTV is not common practice in hydrology, while LSPIV is more frequently adopted in environmental applications. Such a preference depends on PTV requiring high-resolution images that accurately depict tracers and on a priori knowledge of their appearance in the field of view, see also Table 1. In turn, this yields a greater number of input parameters for PTV processing (namely, six input parameters are required in PTVLab against two in PIVLab). While the issue of image resolution was certainly cumbersome in the past, current digital cameras enable impressive resolutions from rather high distances [*Tauro et al.*, 2016d]. Thus, technological advancements facilitate the detection and tracing of extremely small objects for hydrological studies. Finally, the selection of appropriate interrogation windows for LSPIV processing mandates a rather precise knowledge of the size of floating objects and their frame-by-frame displacement. Similar knowledge is also needed for PTV analysis.

Compared to standard PTV practice, filtering reliable trajectories provided tangible data to measure surface velocity. Generally, PTV is based on the development of surface flow velocity maps from the interpolation of trajectory results onto a regularly spaced grid. While such maps are convenient for comparison to LSPIV and numerical simulations, the use of individual trajectories offers a reliable methodology to estimate velocity. Also, applying filters on the trajectories allows for constraining velocity estimation to particles that were correctly detected and tracked by the algorithm. The use of trajectory-based filters is strongly suggested in case of adverse illumination and abundant water reflections, which may bias estimations and lead to fully unrealistic velocities. However, applying the filtering procedure requires a priori information on the flow direction. Even if minimal and based on general common-sense, such information is necessary to provide reliable data, and should be determined on a case-by-case basis. To simplify and automate the identification of flow direction, images could be preliminarily inspected or processed with dimensionality-reduction algorithms [*Tauro et al.*, 2014a].

Based on results on the Brenta and Tiber Rivers and on previous research activities [*Tauro and Grimaldi*, 2017], major causes of inaccuracies in PTV trajectories are due to: i) impossibility to track objects that are not particle-shaped; ii) short frame-by-frame particle displacement with respect to particle dimensions; and iii) massive presence of water reflections that appear as particle-shaped objects in the field of view. Difficulties in detecting and tracking irregularly shaped objects is a crucial limitation of PTVLab and prevents systematic application of PTV in case naturally occurring floaters are used as tracers. This issue should be addressed by designing alternative approaches to identify tracers in images. If particle dimensions are on the same order of magnitude of frame-by-frame displacement, errors in the detection of particle centroids may mask nonlinear deformation of particle patterns [*Brevis et al.*, 2011]. This aspect has a strong influence in fluid regions at high velocity gradients, which are rarely found in hydrological applications, and may be mitigated through image subsampling. The presence of numerous water reflections often results in erroneous trajectories in directions opposite to the flow. Reflections are difficult to remove from images and sometimes require more sophisticated, and costly, equipment. Even if this issue is routinely found in experimental settings, it could be alleviated through extensive trajectory-based filtering and image preprocessing.

Although LSPIV has shown promise in past studies, its reliability is still compromised by particle seeding density and flow unsteadiness. Research efforts to improve the detectability of small objects, and therefore maximize tracer density in the field of view, through advanced image pre-processing are ongoing [*Xu et al.*, 2017]. However, LSPIV limitations hamper a systematic implementation of the technique in practical operational measurements. While LSPIV could still be implemented to provide hydrological data in large scale environments in the vicinity of gauging stations or in locations accessible to operators for tracer deployment [*Legleiter et al.*, 2017], PTV is expected to facilitate the diffusion of remote sensing in hydrological practice by enabling velocity measurements in a wider spectrum of environments. Compared to satellite-based approaches, image sensing indeed offers surface flow velocity field estimations at higher space and time resolutions. In this vein, the combination of PTV and thermal sensing from aerial platforms could significantly advance current knowledge of hydrological processes.

5 Conclusions

In this work, we investigated the relative performance of large scale particle image velocimetry (LSPIV) and particle tracking velocimetry (PTV) towards surface velocity observations in natural streams. We applied standard LSPIV and a modified trajectory-based filtered PTV algorithm to a data set of 12 videos of a small scale stream where tracers were continuously and evenly distributed. Further, we tested the algorithms on a video of a high flow event in the Tiber River, Rome, Italy. In both experimental settings, LSPIV underestimated velocities while PTV was in closer agreement with benchmark data.

Future studies should focus on the ameliorations of PTV. We envision two major research directions towards the development of a less user-assisted and more robust PTV-based methodology for hydrological applications. Firstly, the detection algorithm should afford identification of objects of diverse shapes, dimensions, and pixel intensity. Ideally, the algorithm should be able to automatically recognize every moving object captured in the field of view. Secondly, the trajectory-based filtering procedure should be autonomously implemented to guarantee accurate velocity estimations. In our vision, a set of rules should be developed to automatically discriminate tracers from water reflections and noise. Identification of consistently moving objects could also enhance tracer detection in particularly challenging conditions, such as intense sunlight and water ripples.

Acknowledgments

This work was supported by POR-FESR 2014âĂŞ2020 n. 737616 INFRASAFE, by the UNESCO Chair in Water Resources Management and Culture, and by Fondi ricerca scientifica di Ateneo - Linea B 2016 from University of Tuscia. The authors gratefully thank Andrea Petroselli for support and help with the experiments, and Centro Funzionale âĂŞ Regione Lazio for radar data availability. Quinn Lewis, Salvatore Manfreda, and two anonymous reviewers are acknowledged for insightful comments that have contributed to improve the manuscript. The authors declare no conflicts of interest. Supporting video files and current meter data can be found at doi:10.4121/uuid:940c47ef-fb3b-4191-aabf-6c1d2f781698.

References

Adrian, R. J. (1991), Particle-imaging techniques for experimental fluid-mechanics, *Annual Review of Fluid Mechanics*, *23*, 261–304, doi:10.1146/annurev.fl.23.010191.001401.

Adrian, R. J. (2005), Twenty years of particle image velocimetry, *Experiments in Fluids*, *39*(2), 159 –169, doi:10.1007/s00348-005-0991-7.

Aleixo, R., S. Soares-Frazão, and Y. Zech (2011), Velocity-field measurements in a dam-break flow using a PTV Voronoï imaging technique, *Experiments in Fluids*, *50*(6), 1633–1649, doi:10.1007/s00348-010-1021-y.

Bechle, A., C. Wu, W. Liu, and N. Kimura (2012), Development and application of an automated river-estuary discharge imaging system, *Journal of Hydraulic Engineering*, *138*(4), 327–339, doi:10.1061/(ASCE)HY.1943-7900.0000521.

Bradley, A. A., A. Kruger, E. A. Meselhe, and M. V. I. Muste (2002), Flow measurement in streams using video imagery, *Water Resources Research*, *38*(12), 1–8, doi:10.1029/2002WR001317.

Brevis, W., Y. Niño, and G. H. Jirka (2011), Integrating cross-correlation and relaxation algorithms for particle tracking velocimetry, *Experiments in Fluids*, *50*(1), 135–147, doi:10.1007/s00348-010-0907-z.

Clarke, T. R. (1999), Uncertainty in the estimation of mean annual flood due to rating-curve indefinition, *Journal of Hydrology*, *222*(1–4), 185–190, doi:10.1016/S0022-1694(99)00097-9.

Costa, J., K. Spicer, R. Cheng, F. Haeni, N. Melcher, E. Thurman, W. Plant, and W. Keller (2000), Measuring stream discharge by non-contact methods – a proof-of-concept experiment, *Geophysical Research Letters*, *27*(4), 553–556, doi:10.1029/1999GL006087.

Costa, J. E., R. T. Cheng, F. P. Haeni, N. Melcher, K. R. Spicer, E. Hayes, W. Plant, K. Hayes, C. Teague, and D. Barrick (2006), Use of radars to monitor stream discharge by noncontact methods, *Water Resources Research*, *42*(7), W07,422, doi:10.1029/2005WR004430.

Creëlle, S., R. Roldan, A. Herremans, D. Meire, K. Buis, P. Meire, T. Van Oyen, T. De Mulder, and P. Troch (2016), Validation of large-scale particle image velocimetry to acquire free-surface flow fields in vegetated rivers, *Journal of Applied Water Engineering and Research*, pp. 1–12, doi:10.1080/23249676.2016.1251856, In press.

Creutin, J. D., M. Muste, A. A. Bradley, S. C. Kim, and A. Kruger (2003), River gauging using PIV techniques: a proof of concept experiment on the Iowa River, *Journal of Hydrology*, *277*(3-4), 182–194, doi:10.1016/S0022-1694(03)00081-7.

Detert, M., and V. Weitbrecht (2015), A low-cost airborne velocimetry system: proof of concept, *Journal of Hydraulic Research*, *53*(4), 532–539.

DiBaldassarre, G., and A. Montanari (2009), Uncertainty in river discharge observations: a quantitative analysis, *Hydrology and Earth System Sciences*, *13*(6), 913–921, doi:10.5194/hess-13-913-2009.

Dobson, D. W., K. T. Holland, and J. Calantoni (2014), Fast, large-scale, particle image velocimetry-based estimation of river surface velocity, *Computers & Geosciences*, *70*, 35–43, doi:10.1016/j.cageo.2014.05.007.

Domeneghetti, A. (2016), On the use of SRTM and altimetry data for flood modeling in data-sparse regions, *Water Resources Research*, *52*(4), 2901–2918, doi:10.1002/2015WR017967.

Domeneghetti, A., A. Tarpanelli, L. Brocca, S. Barbetta, T. Moramarco, A. Castellarin, and A. Brath (2014), The use of remote sensing-derived water surface data for hydraulic model calibration, *Remote Sensing of Environment*, *149*, 130–141, doi:10.1016/j.rse.2014.04.007.

Dramais, G., J. LeCoz, B. Camenen, and A. Hauet (2011), Advantages of a mobile LSPIV method for measuring flood discharges and improving stage-discharge curves, *Journal of Hydro-Environment Research*, *5*(4), 301–312, doi:10.1016/j.jher.2010.12.005.

Forsyth, D. A., and J. Ponce (2011), *Computer Vision: a Modern Approach*, Prentice Hall, NJ.

Fujita, I., and Y. Kunita (2011), Application of aerial LSPIV to the 2002 flood of the Yodo River using a helicopter mounted high density video camera, *Journal of Hydro-Environment Research*, *5*(4), 323 – 331, doi:10.1016/j.jher.2011.05.003.

Fujita, I., M. Muste, and A. Kruger (1997), Large-scale particle image velocimetry for flow analysis in hydraulic engineering applications, *Journal of Hydraulic Research*, *36*(3), 397–414, doi:10.1080/00221689809498626.

Fujita, I., H. Watanabe, and R. Tsubaki (2007), Development of a non-intrusive and efficient flow monitoring technique: the space-time image velocimetry (STIV), *International Journal of River Basin Management*, *5*(2), 105–114, doi:10.1080/15715124.2007.9635310.

Gleason, C. J., and L. C. Smith (2014), Toward global mapping of river discharge using satellite images and at-many-stations hydraulic geometry, *Proceedings of the National Academy of Sciences of the United States of America*, *111*(13), 4788–4791, doi:10.1073/pnas.1317606111.

Gleick, P. H. (1998), Water in crisis: paths to sustainable water use, *Ecological Applications*, *8*(3), 571–579, doi:10.1890/1051-0761(1998)008[0571:WICPTS]2.0.CO;2.

Gunawan, B., X. Sun, M. Sterling, K. Shiono, R. Tsubaki, P. Rameshwaran, D. Knight, J. Chandler, X. Tang, and I. Fujita (2012), The application of LS-PIV to a small irregular river for inbank and overbank flows, *Flow Measurement and Instrumentation*, *24*, 1 – 12, doi:10.1016/j.flowmeasinst.2012.02.001.

Hannah, D. M., S. Demuth, H. A. J. van Lanen, U. Looser, C. Prudhomme, G. Rees, K. Stahl, and L. M. Tallaksen (2011), Large-scale river flow archives: importance, current status and future needs, *Hydrological Processes*, *25*(7), 1191–1200, doi:10.1002/hyp.7794.

Hassan, Y. A., and R. E. Canaan (1991), Full-field bubbly flow velocity measurements using a multiframe particle tracking technique, *Experiments in Fluids*, *12*(1), 49–60.

Hauet, A., A. Kruger, W. Krajewski, A. Bradley, M. Muste, J. Creutin, and M. Wilson (2008a), Experimental system for real-time discharge estimation using an image-based method, *Journal of Hydrologic Engineering*, *13*(2), 105–110, doi:10.1061/(ASCE) 1084-0699(2008)13:2(105).

Hauet, A., J. D. Creutin, and P. Belleudy (2008b), Sensitivity study of large-scale particle image velocimetry measurement of river discharge using numerical simulation, *Journal of Hydrology*, *349*(1-2), 178 – 190, doi:10.1016/j.jhydrol.2007.10.062.

Hauet, A., M. Muste, and H.-C. Ho (2009), Digital mapping of riverine waterway hydrodynamic and geomorphic features, *Earth Surface Processes and Landforms*, *34*(2), 242–252, doi:10.1002/esp.1709.

Hauet, A., J.-B. Faure, J. Le Coz, and M. Jodeau (2017), Fudaa-LSPIV version 1.5.1, https://forge.irstea.fr/projects/fudaa-lspiv.

Hoitink, A. J. F., F. A. Buschman, and B. Vermeulen (2009), Continuous measurements of discharge from a horizontal acoustic Doppler current profiler in a tidal river, *Water Resources Research*, *45*(11), W11,406, doi:10.1029/2009WR007791.

International Organization for Standardization (2007a), *ISO 1088:2007. Hydrometry – Velocity-area methods using current-meters – Collection and processing of data for determination of uncertainties in flow measurement*.

International Organization for Standardization (2007b), *ISO 748:2007. Hydrometry – Measurement of liquid flow in open channels using current-meters or floats*.

International Organization for Standardization (2012), *ISO/TR 24578:2012. Hydrometry – Acoustic Doppler profiler – Method and application for measurement of flow in open channels*.

Jodeau, M., A. Hauet, A. Paquier, J. Le Coz, and G. Dramais (2008), Application and evaluation of LS-PIV technique for the monitoring of river surface velocities in high flow conditions, *Flow Measurement and Instrumentation*, *19*(2), 117–127, doi:10.1016/j.flowmeasinst.2007.11.004.

Kähler, C. J., S. Scharnowski, and C. Cierpka (2012), On the uncertainty of digital PIV and PTV near walls, *Experiments in Fluids*, *52*(6), 1641–1656.

Kantoush, S. A., A. J. Schleiss, T. Sumi, and M. Murasaki (2011), LSPIV implementation for environmental flow in various laboratory and field cases, *Journal of Hydro-environment Research*, *5*(4), 263 – 276, doi:10.1016/j.jher.2011.07.002.

Keane, R. D., and R. J. Adrian (1990), Optimization of particle image velocimeters. Part I: Double pulsed systems, *Measurement Science and Technology*, *1*(11), 1202–1215.

Kim, Y. (2006), Uncertainty analysis for non-intrusive measurement of river discharge using image velocimetry, Ph.D. thesis, Graduate College of the University of Iowa.

Kim, Y., M. Muste, A. Hauet, W. F. Krajewski, A. Kruger, and A. Bradley (2008), Stream discharge using mobile large-scale particle image velocimetry: A proof of concept, *Water Resources Research*, *44*(9), W09,502, doi:10.1029/2006WR005441.

Kimura, N., W.-C. Liu, C. H. Wu, A. J. Bechle, W.-B. Chen, and W.-C. Huang (2011), Flow measurement with multi-instrumentation in a tidal-affected river, *Water and Environment Journal*, *25*(4), 563–572, doi:10.1111/j.1747-6593.2011.00257.x.

Koblinsky, C. J., R. T. Clarke, A. C. Brenner, and H. Frey (1993), Measurement of river level variations with satellite altimetry, *Water Resources Research*, *29*(6), 1839–1848, doi:10.1029/93WR00542.

Le Coz, J., G. Pierrefeu, and A. Paquier (2008), Evaluation of river discharges monitored by a fixed side-looking doppler profiler, *Water Resources Research*, *44*(4), W00D09, doi: 10.1029/2008WR006967.

Le Coz, J., B. Blanquart, K. Pobanz, G. Dramais, G. Pierrefeu, A. Hauet, and A. Despax (2016), Estimating the uncertainty of streamgauging techniques using in situ collaborative interlaboratory experiments, *Journal of Hydraulic Engineering*, *142*(7), 04016,011.

LeBoursicaud, R., L. Pénard, A. Hauet, F. Thollet, and J. LeCoz (2015), Gauging extreme floods on YouTube: application of LSPIV to home movies for the post-event determination of stream discharges, *Hydrological Processes*, doi:10.1002/hyp.10532.

LeCoz, J., A. Hauet, G. Pierrefeu, G. Dramais, and B. Camenen (2010), Performance of image-based velocimetry LSPIV applied to flash-flood discharge measurements in mediterranean rivers, *Journal of Hydrology*, *394*(1–2), 42–52, doi:10.1016/j.jhydrol.2010.05.049.

LeCoz, J., B. Camenen, X. Peyrard, and G. Dramais (2012), Uncertainty in open-channel discharges measured with the velocity-area method, *Flow Measurement and Instrumentation*, *26*, 18–29, doi:10.1016/j.flowmeasinst.2012.05.001.

LeCoz, J., A. Patalano, D. Collins, N. F. Guillén, C. M. García, G. M. Smart, J. Bind, A. Chiaverini, R. LeBoursicaud, G. Dramais, and I. Braud (2016), Crowdsourced data for flood hydrology: feedback from recent citizen science projects in Argentina, France, and New Zealand, *Journal of Hydrology*, *541*(Part B), 766–777, doi:10.1016/j.jhydrol.2016.07.036.

Lee, M.-C., C.-J. Lai, J.-M. Leu, W. J. Plant, W. C. Keller, and K. Hayes (2002), Non-contact flood discharge measurements using an X-band pulse radar (I) theory, *Flow Measurement and Instrumentation*, *13*(5–6), 265–270, doi:10.1016/S0955-5986(02)00048-1.

Legleiter, C. J., P. J. Kinzel, and J. M. Nelson (2017), Remote measurement of river discharge using thermal particle image velocimetry (PIV) and various sources of bathymetric information, *Journal of Hydrology*, doi:10.1016/j.jhydrol.2017.09.004, In press.

Lewis, Q. W., and B. L. Rhoads (2015), Resolving two-dimensional flow structure in rivers using large-scale particle image velocimetry: an example from a stream confluence, *Water Resources Research*, *51*(10), 7977–7994, doi:10.1002/2015WR017783.

Li, D.-X., Q. Zhong, M.-Z. Yu, and X.-K. Wang (2013), Large-scale particle tracking velocimetry with multi-channel CCD cameras, *International Journal of Sediment Research*, *28*(1), 103–110, doi:10.1016/S1001-6279(13)60022-0.

Lim, J. S. (1990), *Two-Dimensional Signal and Image Processing*, Prentice Hall, Englewood Cliffs, NJ.

Lloyd, P. M., P. K. Stansby, and D. J. Ball (1995), Unsteady surface-velocity field measurement using particle tracking velocimetry, *Journal of Hydraulic Research*, *33*(4), 519–534, doi:10.1080/00221689509498658.

McMillan, H., J. Freer, F. Pappenberger, T. Krueger, and M. Clark (2010), Impacts of uncertain river flow data on rainfall-runoff model calibration and discharge predictions, *Hydrological Processes*, *24*(10), 1270–1284, doi:10.1002/hyp.7587.

Melcher, N. B., J. E. Costa, F. P. Haeni, R. T. Cheng, E. M. Thurman, M. Buursink, K. R. Spicer, E. Hayes, W. J. Plant, W. C. Keller, and K. Hayes (2002), River discharge measurements by using helicopter-mounted radar, *Geophysical Research Letters*, *29*(22), 2084, doi:10.1029/2002GL015525.

Meselhe, E. A., T. Peeva, and M. V. I. Muste (2004), Large scale particle image velocimetry for low velocity and shallow water flows, *Journal of Hydrologic Engineering*, *130*(9), 937–940, doi:10.1061/(ASCE)0733-9429(2004)130:9(937).

MOBOTIX (2017), *S15 FlexMount Camera*, www.mobotix.com, Kaiserstrasse, Germany.

Moroni, M., and J. H. Cushman (2001), Three-dimensional particle tracking velocimetry studies of the transition from pore dispersion to Fickian dispersion for homogeneous porous media, *Water Resources Research*, *37*(4), 873–884, doi:10.1029/2000WR900364.

Mueller, D. S., C. R. Wagner, M. S. Rehmel, K. A. Oberg, and F. Rainville (2013), *U.S. Geological Survey Techniques and Methods*, vol. A22, chap. Measuring Discharge with Acoustic Doppler Current Profilers from a Moving Boat, p. 95, USGS.

Muste, M., Z. Xiong, J. Schöne, and Z. Li (2004), Validation and extension of image velocimetry capabilities for flow diagnostics in hydraulic modeling, *Journal of Hydraulic Engineering*, *130*(3), 175–185, doi:10.1061/(ASCE)0733-9429(2004)130:3(175).

Muste, M., I. Fujita, and A. Hauet (2008), Large-scale particle image velocimetry for measurements in riverine environments, *Water Resources Research*, *44*(4), W00D19, doi:10.1029/2008WR006950.

Muste, M., H.-C. Ho, and D. Kim (2011), Considerations on direct stream flow measurements using video imagery: Outlook and research needs, *Journal of Hydro-environment Research*, *5*(4), 289 – 300, doi:10.1016/j.jher.2010.11.002.

Nezu, I., and M. Sanjou (2011), PIV and PTV measurements in hydro-sciences with focus on turbulent open-channel flows, *Journal of Hydro-environment Research*, *5*(4), 215–230, doi:10.1016/j.jher.2011.05.004.

Nobach, H., and M. Honkanen (2005), Two-dimensional Gaussian regression for sub-pixel displacement estimation in particle image velocimetry or particle position estimation in particle tracking velocimetry, *Experiments in Fluids*, *38*(4), 511–515, doi:10.1007/s00348-005-0942-3.

Ohmi, K., and H.-Y. Li (2000), Particle-tracking velocimetry with new algorithms, *Measurement Science and Technology*, *11*(6), 603–616, doi:10.1088/0957-0233/11/6/303.

Osorio-Cano, J. D., A. F. Osorio, and R. Medina (2013), A method for extracting surface flow velocities and discharge volumes from video images in laboratory, *Flow Measurement and Instrumentation*, *33*, 188–196, doi:10.1016/j.flowmeasinst.2013.07.009.

Perks, M. T., A. J. Russell, and A. R. G. Large (2016), Technical Note: Advances in flash flood monitoring using unmanned aerial vehicles (UAVs), *Hydrology and Earth System Sciences*, *20*(10), 4005–4015, doi:10.5194/hess-20-4005-2016.

Plant, W. J., W. C. Keller, and K. Hayes (2005), Measurement of river surface currents with coherent microwave systems, *IEEE Transactions on Geoscience and Remote Sensing*, *43*(6), 1242–1257, doi:10.1109/TGRS.2005.845641.

Puleo, J. A., T. E. McKenna, K. T. Holland, and J. Calantoni (2012), Quantifying riverine surface currents from time sequences of thermal infrared imagery, *Water Resources Research*, *48*(1), W01,527, doi:10.1029/2011WR010770.

Raffel, M., C. E. Willert, S. T. Wereley, and J. Kompenhans (2007), *Particle Image Velocimetry. A practical guide.*, Springer, New York.

Ran, Q.-H., W. Li, Q. Liao, H.-L. Tang, and M.-Y. Wang (2016), Application of an automated LSPIV system in a mountainous stream for continuous flood flow measurements, *Hydrological Processes*, *30*(17), 3014–3029, doi:10.1002/hyp.10836.

Scarano, F., and M. L. Riethmuller (2000), Advances in iterative multigrid PIV image processing, *Experiments in Fluids*, *29*(Supplement 1), S051–S060, doi:10.1007/s003480070007.

Schumann, G. J.-P., and A. Domeneghetti (2016), Exploiting the proliferation of current and future satellite observations of rivers, *Hydrological Processes*, *30*(16), 2891–2896, doi:10.1002/hyp.10825.

Smith, L. C. (1997), Satellite remote sensing of river inundation area, stage, and discharge: a review, *Hydrological Processes*, *11*(10), 1427–1439, doi:10.1002/(SICI)1099-1085(199708)11:10<1427::AID-HYP473>3.0.CO;2-S.

Stumpf, A., E. Augereau, C. Delacourt, and J. Bonnier (2016), Photogrammetric discharge monitoring of small tropical mountain rivers: a case study at Rivière des Pluies, Réunion Island, *Water Resources Research*, *52*(6), 4550–4570, doi:10.1002/2015WR018292.

Sveen, J. K. (2004), MatPIV version 1.7.

Tang, H. W., C. Chen, H. Chen, and J. T. Huang (2008), An improved PTV system for large-scale physical river model, *Journal of Hydrodynamics*, *20*(6), 669–678, doi:10.1016/S1001-6058(09)60001-9.

Tarpanelli, A., S. Barbetta, L. Brocca, and T. Moramarco (2013), River discharge estimation by using altimetry data and simplified flood routing modeling, *Remote Sensing*, *5*(9), 4145–4162, doi:10.3390/rs5094145.

Tarpanelli, A., L. Brocca, S. Barbetta, M. Faruolo, T. Lacava, and T. Moramarco (2015), Coupling MODIS and radar altimetry data for discharge estimation in poorly gauged river basins, *IEEE Journal of Selected Topics in Applied Earth Observations and Remote Sensing*, *8*(1), 141–148, doi:10.1109/JSTARS.2014.2320582.

Tauro, F., and S. Grimaldi (2017), Ice dices for monitoring stream surface velocity, *Journal of Hydro-environment Research*, *14*, 143–149, doi:10.1016/j.jher.2016.09.001.

Tauro, F., and S. Salvatori (In press), Surface flows from images: ten days of observations from the Tiber River gauge-cam station, *Hydrology Research*, doi:10.2166/nh.2016.302.

Tauro, F., S. Grimaldi, and M. Porfiri (2014a), Unraveling flow patterns through nonlinear manifold learning, *PLoS ONE*, *9*(3), e91,131, doi:10.1371/journal.pone.0091131.

Tauro, F., M. Porfiri, and S. Grimaldi (2014b), Orienting the camera and firing lasers to enhance large scale particle image velocimetry for streamflow monitoring, *Water Resources Research*, *50*(9), 7470–7483, doi:10.1002/2014WR015952.

Tauro, F., C. Pagano, P. Phamduy, S. Grimaldi, and M. Porfiri (2015), Large scale particle image velocimetry from an unmanned aerial vehicle, *IEEE/ASME Transactions on Mechatronics*, *20*(6), 3269–3275, doi:10.1109/TMECH.2015.2408112.

Tauro, F., A. Petroselli, M. Porfiri, L. Giandomenico, G. Bernardi, F. Mele, D. Spina, and S. Grimaldi (2016a), A novel permanent gauge-cam station for surface-flow observations on the Tiber River, *Geoscientific Instrumentation Methods and Data Systems*, *5*(1), 241–251, doi:10.5194/gi-5-241-2016.

Tauro, F., A. Petroselli, and E. Arcangeletti (2016b), Assessment of drone-based surface flow observations, *Hydrological Processes*, *30*(7), 1114–1130, doi:10.1002/hyp.10698.

Tauro, F., G. Olivieri, A. Petroselli, M. Porfiri, and S. Grimaldi (2016c), Flow monitoring with a camera: A case study on a flood event in the Tiber River, *Environmental Monitoring and Assessment*, *188*(2), 1–11, doi:10.1007/s10661-015-5082-5.

Tauro, F., M. Porfiri, and S. Grimaldi (2016d), Surface flow measurements from drones, *Journal of Hydrology*, *540*, 240–245, doi:Surfaceflowmeasurementsfromdrones.

Thielicke, W., and E. J. Stamhuis (2014), PIVlab - Towards user-friendly, affordable and accurate digital particle image velocimetry in MATLAB, *Journal of Open Research Software*, *2*(e30), 1–10, doi:10.5334/jors.bl.

Tourian, M. J., A. Tarpanelli, O. Elmi, T. Qin, L. Brocca, T. Moramarco, and N. Sneeuw (2016), Spatiotemporal densification of river water level time series by multimission satellite altimetry, *Water Resources Research*, *52*(2), 1140–1159, doi:10.1002/2015WR017654.

Tsubaki, R., I. Fujita, and S. Tsutsumi (2011), Measurement of the flood discharge of a small-sized river using an existing digital video recording system, *Journal of Hydro-environment Research*, *5*(4), 313–321, doi:10.1016/j.jher.2010.12.004.

Turnipseed, D. P., and V. B. Sauer (2010), *U.S. Geological Survey Techniques and Methods*, vol. A8, chap. Discharge Measurements at Gaging Stations, p. 87, USGS.

Uijttewaal, W. S. J., D. Lehmann, and A. vanMazijk (2001), Exchange processes between a river and its groyne fields: model experiments, *Journal of Hydraulic Engineering*, *127*(11), 928–936, doi:10.1061/(ASCE)0733-9429(2001)127:11(928).

van de Giesen, N., R. Hut, and J. Selker (2014), The Trans-African Hydro-Meteorological Observatory (TAHMO), *Wiley Interdisciplinary Reviews: Water*, *1*(4), 341–348, doi: 10.1002/wat2.1034.

Weitbrecht, V., G. Kühn, and G. H. Jirka (2002), Large scale PIV-measurements at the surface of shallow water flows, *Flow Measurement and Instrumentation*, *13*(5-6), 237–245, doi:10.1016/S0955-5986(02)00059-6.

Westerweel, J., and F. Scarano (2005), Universal outlier detection for PIV data, *Experiments in Fluids*, *39*(6), 1096–1100, doi:10.1007/s00348-005-0016-6.

Wu, Q. X., and D. Pairman (1995), A relaxation labeling technique for computing sea surface velocities from sea surface temperature, *IEEE Transactions on Geoscience and Remote Sensing*, *33*(1), 216–220, doi:10.1109/36.368206.

Xu, M., Q. Sun, C. Huang, and J. Shi (2017), Object motion detection and data processing in large-scale particle image velocimetry, *Intelligent Automation & Soft Computing*, doi: 10.1080/10798587.2017.1316080, in press.

Yan, K., A. Tarpanelli, G. Balint, T. Moramarco, and G. DiBaldassarre (2015), Exploring the potential of SRTM topography and radar altimetry to support flood propagation modeling: Danube case study, *Journal of Hydrologic Engineering*, *20*(2), 1–7, doi: 10.1061/(ASCE)HE.1943-5584.0001018.

Yorke, T. H., and K. A. Oberg (2002), Measuring river velocity and discharge with acoustic Doppler profilers, *Flow Measurement and Instrumentation*, *13*(5–6), 191–195, doi: 10.1016/S0955-5986(02)00051-1.

Yossef, M. F. M., and H. J. deVriend (2011), Flow details near river groynes: experimental investigation, *Journal of Hydraulic Engineering*, *137*(5), 504–516, doi:10.1061/(ASCE)HY.1943-7900.0000326.

Yu, K., S. Kim, and D. Kim (2015), Correlation analysis of spatio-temporal images for estimating two-dimensional flow velocity field in a rotating flow condition, *Journal of Hydrology*, *529*(Part 3), 1810–1822, doi:10.1016/j.jhydrol.2015.08.005.